Department of Chemistry and Materials Science

Cycle Life and Recycling of Positive Electrode Materials in Li-Ion Batteries

Katja Lahtinen

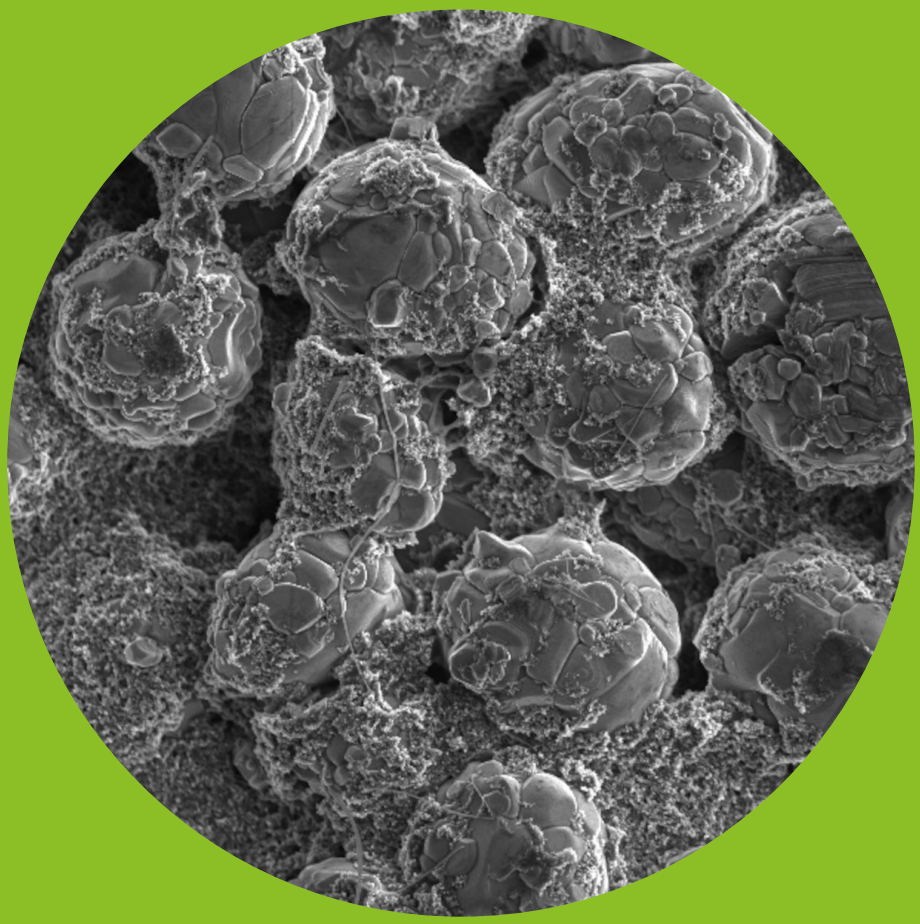

Aalto University

DOCTORAL THESES

Aalto University publication series
DOCTORAL THESES 33/2022

Cycle Life and Recycling of Positive Electrode Materials in Li-Ion Batteries

Katja Lahtinen

A doctoral dissertation completed for the degree of Doctor of Science (Technology) to be defended, with the permission of the Aalto University School of Chemical Engineering, at a public examination held at the lecture hall Ke2 of the School on Chemical Engineering on April 8th 2022 at 12.

Aalto University
School of Chemical Engineering
Department of Chemistry and Materials Science
Research Group of Electrochemical Energy Conversion

Supervising professor
Professor Tanja Kallio, Aalto University, Finland

Thesis advisor
Professor Tanja Kallio, Aalto University, Finland

Preliminary examiners
Assistant professor Stanislav Fedotov, Skolkovo institute of Science and Technology, Russia
Professor Fabio La Mantia, University of Bremen, Germany

Opponent
Associate Professor Reza Younesi, Uppsala University, Sweden

Aalto University publication series
DOCTORAL THESES 33/2022

ISBN 978-952-64-0718-0 (printed)
ISBN 978-952-64-0719-7 (pdf)
ISSN 1799-4934 (printed)
ISSN 1799-4942 (pdf)
http://urn.fi/URN:ISBN:978-952-64-0719-7

Unigrafia Oy
Helsinki 2022

Finland

NORDIC SWAN ECOLABEL
Printed matter
4041-0619

Author
Katja Lahtinen

Name of the doctoral thesis
Cycle Life and Recycling of Positive Electrode Materials in Li-Ion Batteries

Publisher School of Chemical Engineering

Unit Department of Chemistry and Materials Science

Series Aalto University publication series DOCTORAL THESES 33/2022

Field of research Physical Chemistry

Manuscript submitted 15 October 2021 **Date of the defence** 8 April 2022

Permission for public defence granted (date) 26 January 2022 **Language** English

☐ **Monograph** ☒ **Article thesis** ☐ **Essay thesis**

Abstract

Li-ion batteries are a primary power source for portable consumer electronics, such as mobile phones and laptops. In addition, they power electric vehicles (EVs) and can be used as a stationary energy storage for renewable energy sources, such as solar and wind power. Lately, the demand for Li-ion batteries has increased rapidly due to the electrification of transportation, and this has induced challenges related to the sustainability of material production. In this thesis, two major factors in improving the sustainability of Li-ion battery positive electrode materials, cycle life and recycling, are investigated. The thesis focuses on understanding, how dopants or impurities affect the positive electrode materials at the different stages of their life from synthesis to recycling.

First, adding Mg doping to $LiCoO_2$ in different synthesis stages was investigated. Adding the doping in lithiation step was observed to enhance even Mg distribution to the particles and to improve the morphology, which reduced the increase in the charge transfer resistance and led to the improved cycle life. Precursor doping, on the other hand, induced Mg distribution on the particle surface and decreased the stacking order in the crystal, which decreased the cycle life. Li excess in the samples was observed to decrease the rate capability of all the materials regardless the doping stage but not affect the cyclability of lithiation-doped $LiCoO_2$. In addition to doping with a single element, dual doping of $LiCoO_2$ with Mg and Ti was investigated and compared to the Li excess. The Mg-Ti doping was observed to improve the electrochemical performance of $LiCoO_2$ by enhancing the electric conductivity and suppressing the increase of the charge transfer resistance. Li excess was observed to decrease the cycle life in the voltage range of 3.0–4.2 V.

The demand for Li-ion battery raw materials is rapidly increasing alongside the amount of generated waste batteries. In the state-of-art battery recycling processes, all battery parts are recycled at the same process, which leads to impurity metals mixing with the electrode materials. To understand the effect of the metal impurities on the recycling, Li-ion battery waste was recycled using a hydrometallurgical method, and the regenerated chemicals were used in the synthesis of $LiCoO_2$ whose electrochemical performance was then investigated. Cu was observed to be a main impurity in the process, and it decreased the initial capacity of the synthesized materials. However, the regenerated $LiCoO_2$s decreased the increase in impedance, which led to improvements in the rate capability and cycle life.

Alternative methods for the state-of-art recycling methods were discussed as well. In this work, a new method to regenerate spent Li-ion battery positive electrode by electrochemical re-lithiation without removing the active material from the current collector was investigated. The effect of doping on the reusability was investigated as well, and Mg-Ti doping was observed to enhance it. The regenerated materials had a slightly poorer cyclability compared to the fresh materials, which was attributed to the decline in the stacking order and the increase in impedance.

Keywords Li-ion battery, positive electrode material, cycle life, recycling, doping

ISBN (printed) 978-952-64-0718-0 **ISBN (pdf)** 978-952-64-0719-7

ISSN (printed) 1799-4934 **ISSN (pdf)** 1799-4942

Location of publisher Helsinki **Location of printing** Helsinki **Year** 2022

Pages 165 **urn** http://urn.fi/URN:ISBN:978-952-64-0719-7

Aalto-yliopisto

Tiivistelmä

Aalto-yliopisto, PL 11000, 00076 Aalto www.aalto.fi

Tekijä
Katja Lahtinen

Väitöskirjan nimi
Li-ioniakkujen positiivielektrodimateriaalien elinikä ja kierrätys

Julkaisija Kemian tekniikan korkeakoulu

Yksikkö Kemian ja materiaalitieteen laitos

Sarja Aalto University publication series DOCTORAL THESES 33/2022

Tutkimusala Fysikaalinen kemia

Käsikirjoituksen pvm 15.10.2021 **Väitöspäivä** 08.04.2022

Väittelyluvan myöntämispäivä 26.01.2022 **Kieli** Englanti

☐ **Monografia** ☒ **Artikkeliväitöskirja** ☐ **Esseeväitöskirja**

Tiivistelmä

Li-ioniakku on yleisin kannettavassa elektroniikassa, kuten matkapuhelimissa ja kannettavissa tietokoneissa, käytetty akkutyyppi. Lisäksi niitä käytetään energialähteenä sähköajoneuvoissa sekä uusiutuvien energialähteiden, kuten aurinko- ja tuulivoiman, energiavarastoina. Liikenteen sähköistyessä viime aikoina Li-ioniakkujen kysyntä on kasvanut voimakkaasti, mikä on johtanut haasteisiin materiaalien kestävässä tuottamisessa. Tässä työssä tutkitaan kahta Li-ioniakkujen positiivielektrodimateriaalien kestävään tuottamiseen liittyvää tekijää: materiaalien elinikää ja kierrätettävyyttä. Työssä pyritään erityisesti ymmärtämään, miten seostusaineet tai epäpuhtaudet vaikuttavat positiivielektrodimateriaaleihin niiden eri elämänvaiheissa synteesistä kierrätykseen.

Ensimmäiseksi työssä tutkittiin Mg-seostuksen lisäämistä $LiCoO_2$:iin eri synteesivaiheissa. Seostuksen lisäämisen litiointivaiheessa huomattiin edistävän Mg:n jakautumista partikkeleihin tasaisesti sekä parantavan morfologiaa, mikä vähensi materiaalien varauksensiirtovastuksen kasvua ja pidensi elinikää. Prekursorin seostaminen sen sijaan johti Mg:n kerääntymiseen partikkelien pinnoille ja heikensi kiteiden järjestäytyneisyyttä, mikä lyhensi materiaalin elinikää. Näytteiden ylilitioinnin huomattiin heikentävän kaikkien materiaalien suorituskykyä seostuksen lisäämisvaiheesta riippumatta, mutta se ei vaikuttanut litiointivaiheessa seostettujen $LiCoO_2$:n elinikään. Yhden seostusaineen lisäksi työssä tutkittiin myös $LiCoO_2$:n kaksoisseostusta ja sitä verrattiin ylilitiointiin. Mg-Ti-seostuksen huomattiin parantavan $LiCoO_2$:n sähkökemiallista suorituskykyä niin että sähkönjohtavuus lisääntyi ja varauksensiirtovastuksen kasvu pieneni. Ylilitiointi lyhensi elinikää, kun materiaalia ikäännytettiin 3.0–4.2 V jänniteikkunassa.

Li-ioniakkujen raaka-aineiden kysyntä ja akkujätteen määrä kasvaa jyrkästi. Nykyisissä akkukierrätysmenetelmissä kaikki akun osat kierrätetään samassa prosessissa, mikä johtaa elektrodimateriaalien ja epäpuhtausmetallien sekoittumiseen. Metalliepäpuhtauksien kierrätykseen vaikuttavien seikkojen ymmärtämiseksi Li-ioniakkujäte kierrätettiin tässä työssä käyttäen hydrometallurgista kierrätysmenetelmää, ja talteen kerätyt materiaalit käytettiin $LiCoO_2$:n syntetisoimiseen, jonka sähkökemiallista toimintaa tutkittiin. Prosessin pääepäpuhtauden huomattiin olevan Cu, joka laski syntetisoitujen materiaalien alkukapasiteettia. Uudelleensyntetisoidut $LiCoO_2$:t kuitenkin myös laskivat impedanssin kasvua, mikä johti suorituskyvyn ja eliniän paranemiseen.

Vaihtoehtoisia menetelmiä nykyisille kierrätysmenetelmille käsiteltiin myös. Työssä tutkittiin uutta tapaa elvyttää käytettyjä positiivielektrodeja Li-ioniakusta uudelleenlitioimalla ne sähkökemiallisesti ilman aktiivisen materiaalin irrottamista virrankerääjästä. Seostuksen vaikutusta uudelleenkäytettävyyteen tutkittiin myös, ja Mg-Ti-seostuksen huomattiin parantavan sitä. Elvytettyjen materiaalien elinikä oli hieman huonompi kuin tuoreiden materiaalien, minkä pääteltiin johtuvan rakenteen järjestäytyneisyyden heikkenemisestä ja impedanssin kasvusta.

Avainsanat Li-ioniakku, positiivielektrodimateriaali, elinikä, kierrätys, seostus

ISBN (painettu) 978-952-64-0718-0 **ISBN (pdf)** 978-952-64-0719-7

ISSN (painettu) 1799-4934 **ISSN (pdf)** 1799-4942

Julkaisupaikka Helsinki **Painopaikka** Helsinki **Vuosi** 2022

Sivumäärä 165 **urn** http://urn.fi/URN:ISBN:978-952-64-0719-7

Acknowledgements

The work presented in this thesis was conducted in the Research group of Electrochemical Energy Conversion at the Department of Chemistry and Materials Science in Aalto University between 2017 and 2021. The financial support from Aalto CHEM, Academy of Finland (CloseLoop and BatCircle -projects) and Business Finland (B4B-project) is gratefully acknowledged.

I have had the privilege to work with several wonderful people during my doctoral studies. First, I am the most grateful to Prof. Tanja Kallio for introducing me to Li-ions batteries and giving me the opportunity to do the doctoral study in her group. In the beginning of my studies in Aalto University approximately 10 years ago, I had no idea what I wanted to do after graduation. If somebody asked, I usually answered: "something related to the environment and chemistry would be nice, and if there's one thing I want to avoid, it is electrochemistry". Well, I could not avoid the electrochemistry, but working on Li-ion batteries did introduce me to a topic related to my interests. It also showed me that you should never say never – nowadays I quite enjoy electrochemistry. Tanja's group has been a good and safe place to learn, with opportunities and space to grow. Thank you, a lot.

I also want to thank all my co-workers and co-authors for their help, support and contribution to the work presented in this thesis. I am especially grateful to Dr. Taina Rauhala for the instruction and feedback she gave me in the beginning of this work, and Dr. Eeva-Leena Rautama for teaching me crystal refinement and always having time for my questions. Dr. Hua Jiang is acknowledged for the long hours he used to measure all my samples with TEM. I thank all my battery group colleagues, especially Dr. Ekaterina Fedorovskaya, Dr. Seyedabolfazl Mousavi, Xiangze Kong and Zahra Ahaliabadeh, for interesting discussions that have helped me to learn. I have also had the pleasure to instruct several bachelor's and master's thesis workers and research assistants. Thank you for your experimental work in the lab and all the tricky questions that forced me to think.

The environment at CMAT has been wonderful to work at. I give my warmest thanks to everybody who has joined our group's Thursday coffee breaks, I have enjoyed the discussions enormously. I also want to thank everybody working at CMAT at some point of these past years. Many people have helped me at some point, sometimes in seemingly small things, such as organizing the lab waste, emptying the dishwasher, or telling me that there is life after dissertation, which however have made my life easier in those moments. Special thanks in this regard go to Dr. Milla Suominen, Farhan Ali and Janez Kosir. I would also like to acknowledge Anita Pirhonen for her help acquiring the materials and equipment necessary for my experiments, and Dr. Juha Linnekoski for his help with laboratory and glovebox maintenance.

I have also received support outside work. I am grateful for all my friends who have supported me during these past years. I warmly thank Dr. Laura Jakobsson for the countless jogs and lunch breaks we have had together. Her peer support has been irreplaceable during these years of doctoral studies. I would also like to acknowledge a group of friends which I call here “the Corona bubble”. I thank them for keeping me sane during the lockdown period in 2020 and for bringing excitement to my everyday life, be it through a trip to Lapland or an adventure in Anliscia. Special thanks to Maaria Jenu and Meri Sipilä for our sauna sessions and Samppa Jenu for proofreading this work.

Finally and the most importantly, I want to thank my family for their love and support through this process. I thank my siblings Krista, Atte and Riina for all the memories of growing up together. We all have our own lives now, but even after months of being apart, I always feel safe talking to them. Mom and Dad I am eternally grateful to – I wouldn’t be where I am without them. They have always given me space to make my own decisions but lent an understanding ear, given constructive feedback or encouraged me if I wanted it. Thank you for being there for me.

Katja Lahtinen
Espoo, October 2021

Contents

List of Publications

This doctoral dissertation consists of a summary of the following publications which are referred to in the text by their Roman numerals

I K. Lahtinen, M. Labmayr, V. Mäkelä, H. Jiang, J. Lahtinen, L. Yao, E.O. Fedorovskaya, S. Räsänen, S. Huotari, T. Kallio, Long-term cycling behavior of Mg-doped $LiCoO_2$ materials prepared at different doping stages and investigated with the help of laboratory scale X-ray absorption near-edge spectroscopy, *Submitted to Materials Today Energy*

II K. Lahtinen, T. Rauhala, S. Räsänen, E.-L. Rautama, T. Kallio, The effect of synthesis modifications on the lithium cobalt oxide using commercial precursors, *Electrochimica Acta*, **327** (2019) 135012. DOI: 10.1016/j.electacta.2019.135012

III C. Peng, K. Lahtinen, E. Medina, P. Kauranen, M. Karppinen, T. Kallio, B. Wilson, M. Lundström, Role of impurity copper in Li-ion battery recycling to $LiCoO_2$ cathode materials, *The Journal of Power Sources*, **450** (2020) 227630. DOI: 10.1016/j.jpowsour.2019.227630

IV K. Lahtinen, E.-L. Rautama, H. Jiang, S. Räsänen, T. Kallio, Reuse of $LiCoO_2$ Electrodes Collected from Spent Li-Ion Batteries after Electrochemical Re-Lithiation of the Electrode, *ChemSusChem*, **14** (2021) 1-12. DOI: 10.1002/cssc.202100629

Author's Contribution

Publication I: Long term cycling behavior of Mg-doped $LiCoO_2$ materials prepared at different doping stages and investigated with the help of laboratory scale X-ray absorption near-edge spectroscopy

The author defined the research plan together with T.K, S.R, and S.H. and conducted the literature review with E.F. The author performed XRD, SEM, Raman spectroscopy, CV and EIS measurements. The author planned the rate capability and cycling tests and conducted them together with M.L. TEM and EELS measurements were conducted by H.J and the data analyzed by the author while cross-section samples were prepared by L.Y. and the XPS measurements were conducted by J.L. XANES measurements and analysis was done by M.L, V.L. and S.H. The author interpreted the results, wrote the manuscript, and refined it based on the comments by other authors.

Publication II: The effect of synthesis modifications on the lithium cobalt oxide using commercial precursors

The author defined the research plan together with the co-authors (T.K, T.R, S.R, E.R), planned the electrochemical measurements with T.R. and performed them. In addition, the author conducted the XRD and Raman measurements and the analysis of the EELS data. The Rietveld refinements were conducted by E.R., TEM and EELS measurements by Dr. Hua Jiang and SEM measurements by T.R. The author conducted the interpretation of the electrochemical results together with T.R, wrote the manuscript, and refined it according to the comments by the other authors.

Publication III: Role of impurity copper in Li-ion battery recycling to $LiCoO_2$ cathode materials

Conceptualization of the work was done by B.W, T.K, M.K, P.K and M.L, and project management by P.K. Funding acquisition, resources and supervision were provided by M.K, M.L and T.K. Investigation and methodology were conducted by C.P (Leaching, Li and Co recovery), E.M (TGA measurements, synthesis and XRD) and the author (electrochemical measurements, SEM). Writing the original draft, analysis of data and visualization were carried out by C.P, the author and E.M, the author

focusing on the sections related to electrochemistry. All authors participated in reviewing and editing of the manuscript.

Publication IV: Reuse of $LiCoO_2$ Electrodes Collected from Spent Li-Ion Batteries after Electrochemical Re-Lithiation of the Electrode

The author defined the research plan together with T.K. and planned and performed the electrochemical measurements, XRD, Raman spectroscopy, SEM measurements. The TEM and EELS measurements were conducted by H.J, the AAS measurements by Mr. Hannu Revitzer and the Rietveld analysis by E.R. The author interpreted the results, wrote the manuscript, and refined it according to the comments by the other authors (T.R, E.R, H.J, S.R.).

List of Abbreviations and Symbols

AAS	Atomic absorption spectroscopy
CMC	Carboxymethyl cellulose
CNT	Carbon nanotube
CV	Cyclic voltammetry
EC	Ethylene carbonate
EELS	Electron energy loss spectroscopy
EIS	Electrochemical impedance spectroscopy
DEC	Diethyl carbonate
DMC	Dimethyl carbonate
GITT	Galvanostatic intermittent titration technique
ICP-OES	Inductively coupled plasma optical emission spectroscopy
LCO	$LiCoO_2$
LFP	$LiFePO_4$
LMO	$LiMnO_2$
LNO	$LiNiO_2$
LTO	$Li_4Ti_5O_{12}$
NCA	$Li(Ni_xCo_yAl_z)O_2$
NMC	$Li(Ni_xCo_yMn_z)O_2$
NMP	N-methyl-2-pyrrolidone
PAA	Polyacrylic acid
PE	Polyethylene
PP	Polypropylene
PVDF	Polyvinylidene fluoride

SBR	Styrene butadiene
SEI	Solid electrolyte interphase
SEM	Scanning electron microscopy
TEM	Transmission electron microscopy
XANES	X-ray absorption near edge spectroscopy
XPS	X-ray photoelectron spectroscopy
XRD	X-ray spectroscopy

D	Diffusion coefficient
F	Faraday's constant
i	Current
l	Diffusion length
S	Electrode/electrolyte contact area
t	Time
U	Potential, voltage
V_m	Molar volume of the active material
z_A	Charge number
δ	Stoichiometric amount of the atoms moving in the reaction

1. Introduction

Li-ion battery is a secondary battery which utilizes lithium ions to enable charge and discharge of the cell. Its concept is based on the use of electrodes that can take in and store Li-ions without irreversibly damaging the host structure. Based on the research on Li-ion intercalation [1], development of lithium cobalt oxide ($LiCoO_2$) positive electrode [2] and development of a first Li-ion battery cell [3], Li-ion batteries were commercialized by Sony in 1991 [4], and after that they have revolutionized the use of portable consumer electronics. In 2019, Stanley Whittingham, John Goodenough and Akira Yoshino were awarded the Nobel prize in Chemistry for their contribution to the research [5].

Because of the light weight, high energy density, low self-discharge rate and long cycle life, the use of Li-ion batteries as a power source in small devices, such as mobile phones and laptops, became common quickly after their introduction, and today they dominate the market. Recently, the growing awareness of the climate change has led to the efforts to reduce the use of fossil fuels and that way the carbon emissions. In addition to intensified development of renewable energy sources such as solar and wind power, this accelerated the development of electric vehicles (EVs) which are currently powered by Li-ion batteries as well. Li-ion batteries are also an alternative for stationary energy storage systems for the renewable power sources. The growing demand for consumer electronics, and especially for EVs has also increased the demand for Li-ion batteries, which has rapidly increased during the last few years. For example, between 2010 and 2018 the annual increase in demand was 30 %, the volume in 2018 being 180 GWh. In the future the market is expected to continue growing approximately 25 % annually. [6]

The utilization of Li-ion batteries in large scale applications induces new challenges to be solved. For the EVs to compete with internal combustion engine vehicles, several factors such as driving range, lifetime, fast charging, cost and safety should be enhanced. For example, currently the lifespan of the Li-ion battery determines the lifespan of the EV, because the battery is so well integrated to the vehicle that changing it when the battery reaches its end-of-life is unpractical.[7] For the vehicle to stay usable, the battery has to match its expected lifetime. U.S. Advanced Battery Consortium has set a target for EV battery lifespan to be 15 years [8]. In stationary energy storage, good power capability, reliability, safety, cost and lifetime are required of the battery [9], but the energy density can be lower than for mobile applications. Regardless the use and requirements for a Li-ion battery cell, lifetime, or often called cycle life, has a key role determining its cost and impact on the environment. While the price and energy needed to produce a battery cell are often high, a long lifetime increases the total energy stored in the system and lowers the cost and energy spent per energy converted. Long lifetime also increases the time between the cell changes

from old to new, decreasing the demand for new materials. Because of these reasons, investigating battery lifetime and factors to enhance it is important.

In addition to issues concerning the demands for new applications, the growing market is facing challenges related to raw materials and waste management. The rapidly increasing demand is threatening to increase the prices and might even lead to resource shortages of several critical elements for electrode production, such as cobalt and lithium [10,11]. Simultaneously, the Li-ion battery waste management is insufficient. While recycling processes exist, the field is not properly regulated and a large part of the used Li-ion batteries end in landfills [12]. This leads to the loss of valuable metals, and exposes the environment to hazardous chemicals, such as fluorine-containing electrolytes. To protect the environment and to answer the high demand for battery chemicals, recycling offers a logical way to introduce the used materials back to the material flow. However, a Li-ion battery cell consists of several components tightly tied together, and a battery pack for EV may consists of hundreds of cells. This complicates the recycling considerably, and in the current recycling methods this is generally solved by collecting only the most valuable metals. To utilize all the materials in Li-ion battery waste, the recycling processes should be further investigated and developed.

The Li-ion battery properties are determined greatly by the electrode materials. Graphite is the most widely used material in the negative electrode, but lithium titanate ($Li_4Ti_5O_{12}$) and Si-C composites are commercially available as well. In the positive electrode, layered transition metal oxides, such as $LiCoO_2$, $LiNi_xMn_yCo_{1-x-y}O_2$ and $LiNi_{0.8}Co_{0.15}Al_{0.05}O_2$, as well as lithium iron phosphate ($LiFePO_4$) and lithium manganese oxide ($LiMn_2O_4$) are commercially available. Layered transition metal oxides are one of the most popular materials due to high energy density of the Ni-rich and high average voltage of the Co-rich compounds. The stability, safety and lifetime of the layered transition metal oxides can be enhanced with Mn, but this lowers the energy density and good voltage characteristics. One of the most popular ways to modify the electrochemical properties of layered transition metal oxides is doping them with small amounts of other elements.

This thesis focuses on understanding factors that affect the sustainability of layered transition metal oxides, lifetime and recycling. The topic is examined from the point of view of doping with the aim to understand how it affects the different stages of material lifespan: synthesis, performance, recycling, and reuse. $LiCoO_2$ is used as the investigated material. While it is already a well-known material compared to many other layered transition metal oxides, it serves as a good model compound due to its similar but simpler structure.

First, the effect of adding dopant at different synthesis stages is investigated. In solid-state synthesis of $LiCoO_2$, doping is generally added simultaneously with Li and Co-precursors, the last synthesis step sometimes called “lithiation”. However, in electrode material recycling, the active material might be exposed to impurities, some of which are considered performance enhancing in controlled conditions. In Publication I, the conventional lithiation-step doping synthesis is compared to synthesis using Mg-doped Co-precursor to understand how the presence of impurity or dopant in the precursor affects the physical and electrochemical properties of the synthesized material, and whether the removal of the impurities is necessary or not.

Next the thesis focuses on understanding the effect of doping on the cycle life of $LiCoO_2$. While the Mg doping is discussed in Publication I, doping with two cations

simultaneously is examined in Publication II. In addition, the effect of Li/Co stoichiometry on the performance of both doped and non-doped materials is investigated (Publications I and II). Publication II focuses specially to compare the over-stoichiometry with dual doping. The long-term cycling of the materials is done in LCO/graphite pouch cells to understand the behavior of the materials in a real-life setting.

In the second part of the thesis, recycling of layered transition metal oxides is discussed. In the industry, Li-ion batteries are generally recycled without separating the different cell parts. However, the literature on electrode material recycling is mostly focused on recollection of active materials after several separation processes. The lack of separation at the start of recollection leads to mixing of the electrode materials with e.g. current collector and casing metals. In Publication III, the effect of impurities on the recycling process is discussed. Co and Li are collected from the Li-ion battery waste and the recollected Co precursor is observed to contain Cu as an impurity. $LiCoO_2$ is synthesized of the obtained precursors and the effect of the Cu impurity on the electrochemical performance is investigated to learn whether it is necessary to remove all the impurities of the recycled electrode material.

Publication IV scrutinizes the recycling of layered transition metal oxides from another perspective. Typical state-of-the-art electrode material recycling methods consists of several process steps, such as burning, dissolution, precipitation. After all the steps, the electrode material is usually downgraded to precursor material and energy is required to synthesize it back to the original material. Therefore, recycling methods with minimized amount of process steps that do not downgrade the electrode material should be developed. In Publication IV, a new method to regenerate aged positive electrode materials through electrochemical re-lithiation is introduced and investigated to understand whether this method could be utilized in the electrode material recycling in the future. The re-lithiation is done for both Mg-Ti doped and non-doped $LiCoO_2$ to investigate how doping affects the regeneration of the materials.

As a summary, this thesis investigates the effect of doping in all stages of life for layered transition metal oxide electrode materials in Li-ion battery. Especially the lifetime and recycling of the materials are discussed to enhance the sustainability of the materials.

2. Materials in Li-ion batteries

A typical Li-ion battery cell consists of a positive electrode, a negative electrode, and an electrolyte that allows Li-ion transportation but insulates electron transport. In addition, the cell usually has external wiring for electron transport and a separator to avoid short circuit between the positive and negative electrodes [13,14]. The electrodes consist of an active material mixed with possible additives and a current collector. The active electrode materials need to be able to take in and let out Li-ions irreversibly to enable the working of the cell. Often the materials are so-called intercalation compounds whose host material structure does not radically change upon (de)-insertion of Li. However, alloying and conversion reaction based materials are used as well [15].

The operation of a Li-ion battery is based on the Li ions moving between the two electrodes. When the battery is charged, the positive electrode is oxidized, and the Li-ions move through the electrolyte to the negative electrode. Simultaneously, electrons move through external wiring to the negative electrode which is reduced. During discharge, the reactions are reversed. The structure and operating principle of Li-ion battery are presented in Figure 1. In this chapter, typical materials used in Li-ion battery are introduced.

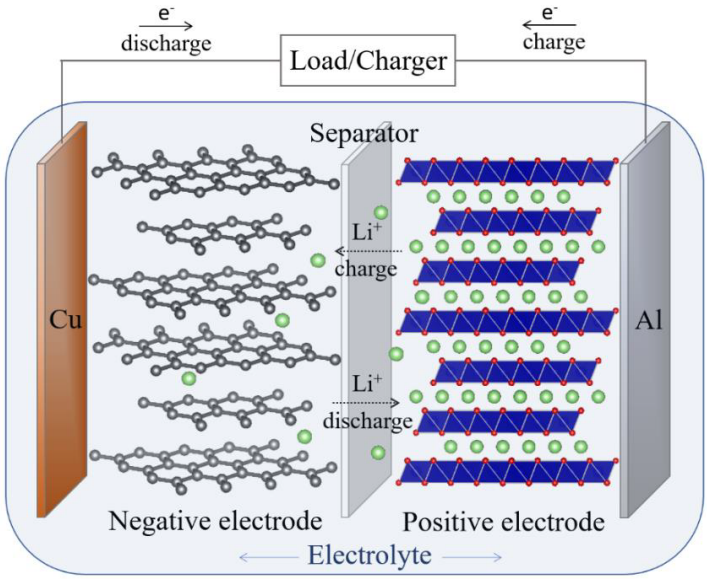

Figure 1. Li-ion battery cell parts and operating principle.

2.1 Positive electrode materials

$LiCoO_2$ was introduced by Goodenough *et al.*[2] in 1980s and it was used in the positive electrode of the first commercial Li-ion battery introduced in 1990[4]. $LiCoO_2$ (LCO) is a layered transition metal oxide with a space group of $R\bar{3}m$. The structure consists of CoO_2-layers stacked along c-axis and layers of Li ions stacked between them[16]. The structure of LCO, along with a few other positive electrode materials, is presented in Figure 2. In a battery, LCO is at its basic form when the cell is in a discharged state. When the battery is charged, Li ions are extracted from the lattice and Co^{3+} is oxidized to Co^{4+}. The reaction is reversed during discharge. LCO has a high operating voltage (3.9 V vs. Li^+/Li), high volumetric energy density, good electrical and ionic conductivities, low self-discharge rate and it is relatively simple to synthetize. It also exhibits a high theoretical capacity of 274 mAh g^{-1}, but in practice, only around 160 mAh g^{-1} can be utilized due to the instability of the crystal structure if too much Li is extracted. The too high Li extraction rate leads to the collapse of the CoO_2-layers and oxygen release. The oxygen reacts with the organic electrolyte, which could potentially lead to a battery fire.[16–18] In addition, Co is expensive and 60 % of it is produced in the Democratic Republic of Congo where the mining conditions are reported to be unethical[19,20].

To avoid the disadvantages of Co, its replacement with other elements have been investigated widely. Soon after introduction of LCO, $LiNiO_2$ (LNO) and $LiMnO_2$ (LMO) were presented. In many ways, Ni and Mn are good options: they are more abundant and cheaper, more environmentally friendly (especially Mn), and have similar theoretical capacity compared to LCO[21]. However, both LNO and LMO are more unstable which has prevented their use in practice. In case of LNO, due to similar size of Li^+ and Ni^{2+}, Ni^{2+} ions replace Li ions in the lattice, which blocks the Li ion diffusion pathways[22]. In case of LMO, its layered structure changes irreversibly to spinel structure during Li extraction[23].

As the complete replacement of Co did not work out, the research focus moved to partial replacement of Co. This proved a good perspective and led to the development of various compounds, most notably $Li(Ni_xCo_yMn_z)O_2$ (NMC)[24] and $Li(Ni_xCo_yAl_z)O_2$ (NCA)[25] which the current electric vehicle batteries are based on. NMC structure can be described as a solid solution of LNO, LCO and LMO with the transition metal valence states being 2+, 3+ and 4+ for Ni, Co, and Mn, respectively. When the cell is charged, Ni^{2+} is oxidized to Ni^{4+}, Co^{3+} to Co^{4+} and Mn^{4+} remains unchanged.[26,27] NMC has a usable theoretical capacity of 150–200 mAh g^{-1} depending on the voltage window and composition [28]. The first commercially successful NMC material was $LiNi_{0.33}Co_{0.33}Mn_{0.33}O_2$, which then led to efforts decreasing the amount of Co to reduce the material costs [29]. Nowadays $LiNi_{0.6}Co_{0.2}Mn_{0.2}O_2$ is the most common NMC material commercially while $LiNi_{0.8}Co_{0.1}Mn_{0.1}O_2$ is under intense research [30]. However, while increasing the amount of Co does lower the price of the transition metal oxide, the Ni-rich materials are often more unstable.

An alternative to NMC compounds is the NCA compounds of which $LiNi_{0.8}Co_{0.15}Al_{0.05}O_2$ is the most common. It has the usable theoretical capacity of approximately 200 mAh g^{-1} and average operating potential of 3.7 V vs. Li^+/Li, similarly to NMC. During the cell charge, Ni^{3+} oxidizes to Ni^{4+}, Co^{3+} to Co^{4+} and Al^{3+} is inactive [28]. While the cycle life of NCA is good at normal conditions, the capacity fade has been shown to be more severe at elevated temperatures (40–70 °C). This is

caused by the thickening of cathode electrolyte interphase (CEI) layer and formation of microcracks in the grain boundaries. [31] Tesla electric vehicles reportedly use Panasonic NCA batteries [32].

To increase the positive electrode capacity, lithium-rich layered oxides have been investigated as well. In these materials the excess Li either replaces part of transition metals in the transition metal layer[33] or an additional phase of Li_2MnO_3 is added to the layered oxide structure [34]. These materials can achieve a high theoretical capacity of >200 mAh g^{-1} and the Li_2MnO_3 acts as a Li reservoir. However, they usually have a high first cycle irreversible capacity loss and poor cycle life [32].

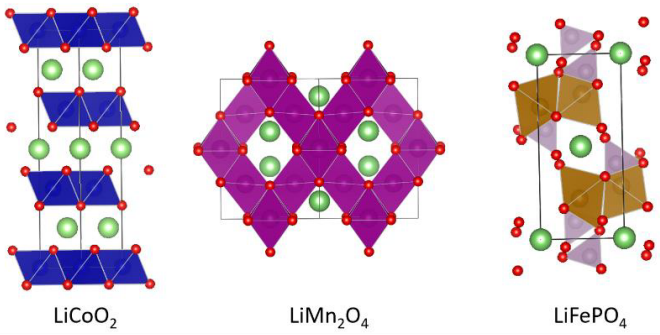

Figure 2. Positive electrode materials in Li-ion batteries

The layered transition metal oxides discussed above have been dubbed as "two-dimensional" materials due to their layered nature. In addition to them, alternative "three-dimensional" structures have been investigated as well. Similarly to $LiMnO_2$, spinel-structured $LiMn_2O_4$ has the advantages of low cost, environmentally friendliness and good thermal stability due to use of Mn. In the structure, manganese oxide forms a three-dimensional framework and Li can diffuse through interstitial pathways [35]. $LiMn_2O_4$ has a high average operation potential of 4.1 V vs. Li^+/Li but its usable theoretical capacity is relatively low, being only 120 mAh g^{-1}. In addition, $LiMn_2O_4$ has a quite poor cycling stability due to volume changes and Jan-Teller distortion of Mn^{3+} at low voltages. In addition, Mn^{3+} can undergo a disproportionation reaction to form Mn^{4+} and Mn^{2+}. Mn^{2+} dissolves easily to the electrolyte and drifts to graphite negative electrode solid electrolyte interphase (SEI) layer destabilizing it [36,37]. $LiMn_2O_4$ has been commercialized, but it is mostly used in mixtures with transitional metal oxides to enhance the battery cycle life and price [38].

Polyanion compounds are a group of three-dimensional materials, and olivine $LiFePO_4$ (LFP) is the most well-known material within this group. Its structure consists of connected PO_4 tetrahedra and FeO_6 octahedra that form a framework. Then, similarly to $LiMn_2O_4$, Li diffuses in the material through interstitial pathways [39–41]. When LFP is charged, a two-phase reaction occurs between lithiated $LiFePO_4$ and de-lithiated $FePO_4$ with iron oxidation state simultaneously changing from Fe^{2+} to Fe^{3+}. This leads to a very flat voltage profile. LFP has a good thermal stability, cycle life, and relatively good theoretical capacity. It is also environmentally friendly and a low-cost material. However, its average operating potential is only 3.4 V vs. Li^+/Li and the electrical and ionic conductivity are poor [39]. The performance of LFP can be enhanced by reducing the particle size, mixing with conductive materials such as

carbon nanotubes (CNTs) or doping [42–44]. Nevertheless, due to the low operating potential, LFP is mostly used in power applications, energy storage, or in vehicles that do not require high capacity, such as electric busses [45].

2.2 Negative electrode materials

An ideal negative electrode material for Li-ion batteries is metallic Li. It has a very high theoretical capacity of 3860 mAh g^{-1} and the lowest possible negative electrochemical potential of -3.040 V vs. standard hydrogen electrode (or 0 V vs. Li^+/Li) [46]. Therefore, rechargeable Li metal batteries have been investigated widely during the last 40 years. However, there are two major disadvantages in using metallic Li as a negative electrode. First, Li dendrites grow on the electrode surface during repeated charge/discharge processes. A dendrite can puncture through the separator and cause a short circuit in the cell. Second, the coulombic efficiencies of the processes occurring in the cell are low, which leads to a short cycle life. Because of these reasons, metallic Li was mostly discarded in the past and the focus of the research moved to other materials. However, lately the interest in metallic Li has been increasing again due to rise of solid electrolytes which have potential to block the dendrites reaching the positive electrode due to their mechanical strength [47,48].

Carbonaceous materials were introduced in the early stage of Li-ion battery material investigation. Petroleum coke was used in the first commercial applications, but graphitic carbon replaced it soon after [13], and hitherto it has been the most used negative electrode material. Graphitic carbon has a hexagonal layered structure formed by graphene sheets stacked on top of each other. The intercalation of Li in graphite proceeds via a mechanism known as staging in which Li fills the graphene layers in an ordered way, layer by layer, keeping the number of de-lithiated layers between the lithiated layers as large as possible [49,50]. At the end of the lithiation, all layers are filled with up to 1 Li atom per 6 C atoms. Graphitic carbon has several advantages as it is cheap, abundant, non-toxic and has a good electrical conductivity. In addition, the specific capacity is relatively high, being 372 mAh g^{-1} and the operation potential is low (0.1–0.2 V vs. Li^+/Li for different lithiation stages) which enables high voltages for full cells.

The low operation potential of graphite is not only an advantage. Because it is close to the reduction potential of Li, there is a risk of Li deposition and dendrite formation on the electrode at high currents and low temperatures [51–53]. This causes similar risks to use of metallic Li and restricts the use of graphite to milder conditions. In addition, the graphite operation potential is below the stability window of the most commonly used electrolytes. This leads to the reduction and decomposition of the electrolyte on the graphite surface. Many decomposed electrolytes solvate Li ions and intercalate into graphite causing extreme expansion of the graphite structure and leading to the exfoliation and breaking of graphite particles [49,54,55]. For graphite to work as a negative electrode, it is important to use electrolytes that form a passivating layer on it instead of solvating Li ions [55]. The passivating layer is called a solid electrolyte interphase (SEI) layer, and it is the mixture of electrolyte reduction products such as Li_2CO_3, LiF, Li_2O and Li-alkyl carbonates, the exact composition depending on the materials used in the cell [56–59]. SEI layer is ionically conductive, and therefore, it does not prevent Li-ion diffusion through the layer to the graphite necessary for the intercalation [55,59]. On the other hand, it is electrically insulating, preventing the

continuing layer growth. Ideally, SEI layer is formed during the first charge-discharge cycle and after that it stabilizes, preventing the further reduction of the electrolyte. In practice however, the layer slowly thickens with continued aging. The formation of SEI layer consumes Li ions irreversibly from the cell, and it is typically the largest singular cause for Li loss in Li-ion batteries using graphite as a negative electrode.

$Li_4Ti_5O_{12}$ (LTO) is an alternative for graphite. It has a three-dimensional spinel structure, and similarly to LFP and $LiMn_2O_4$, Li can diffuse through the material using interstitial pathways [60]. The LTO structure is presented in Figure 3 alongside the structure of graphite. The volume changes during LTO lithiation/de-lithiation are very small, being only 0.2 %, and because of this it is thermally very stable [60–62]. LTO is also relatively cheap and has a relatively high specific capacity of 175 mAh g^{-1} and a long cycle life. The operation potential of LTO is 1.55 V vs. Li^+/Li. It is higher than graphite's, meaning that it does not enable as high cell voltages as graphite and the specific energy of the cells are low. However, 1.55 V vs. Li^+/Li is well above the electrolyte stability window, and therefore there are no SEI layer formation or Li plating even in high currents or low temperatures [21,63]. This stabilizes the material even more and makes it also very safe to use. LTO is typically used in applications requiring high power.

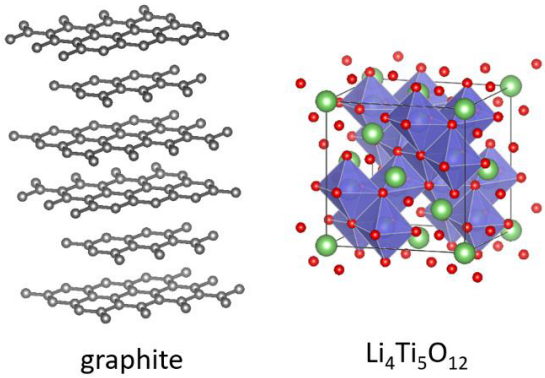

Figure 3. Negative electrode materials in Li-ion batteries

In the search of alternative electrode materials for Li-ion battery, not only Li intercalation materials have been investigated. Materials forming an alloy with Li or changing to another compound entirely when reacting with Li have been investigated as well. The alloy forming materials include elements such Si and Sn. The theoretical capacities of these materials are extremely high, for example 4200 mAh g^{-1} for Si, but they also suffer from large volume changes during cycling[64]. The volume changes cause particle and SEI layer cracking, leading to continuous electrolyte decomposition and loss of Li [65,66]. This makes the alloy forming materials difficult to use alone. However, mixing the alloy materials with carbon has been shown to enhance the stability of the materials. For example, Si particles can be encapsulated in a carbon shell to protect it from SEI formation [67,68]. On the other hand, Si can also be mixed to graphite in small amounts to increase its capacity, and this has become common in the industry [38,69] during the past few years.

Conversion reaction materials are another option for Li intercalation materials. These materials are typically oxides such as MnO, Co_3O_4 and Fe_2O_3 that form Li_2O

when they are lithiated [70,71]. The Li_2O forms a network that keeps the material together [72]. Conversion reaction materials have typically a high theoretical capacity, but the electrical conductivity of Li_2O is low leading to large irreversible capacity losses and high voltage hysteresis. In addition, the volume changes are large too, leading to contact failures, pulverization and SEI layer cracking [70].

2.3 Electrolytes

Electrolyte is an ionically conductive component that allows charge to transfer between two electrodes in an electrochemical cell. It is simultaneously electrically insulative to avoid short circuit and self-discharge of the cell. [73,74] In Li-ion batteries, several different types of electrolytes, such as liquid electrolytes, solid-state electrolytes and gel electrolytes, can be used. While the composition of these different electrolyte types is different, most of them contain Li in some form to allow Li-ion transport within the cell.

Liquid electrolytes are the most used electrolyte type in Li-ion batteries. A typical liquid electrolyte consists of a Li salt such as $LiPF_6$ dissolved in organic carbonates such as ethylene carbonate (EC), propylene carbonate (PC), diethyl carbonate (DEC) and dimethyl carbonate (DMC) [74,75]. Cyclic organic carbonates, e.g. EC and PC, dissolve many Li salts well, and they are therefore necessary for the liquid electrolytes. EC is the most used one due its good SEI layer forming properties [38,76]. On the other hand, the viscosity and melting point of cyclic organic carbonates are high and because of this they are often mixed with acyclic alkyl carbonates, such as DEC and DMC, for lower values [73,75]. However, the boiling and flash points of acyclic alkyl carbonates are quite low, and this limits the safety range of the cell. The performance of liquid electrolytes can also be enhanced using additives such as vinylene carbonate (VC). An additive can be used for example to enhance the surface layer formation, sometimes in a sacrificial way [75].

Due to the limited safety of liquid electrolytes, a lot of effort has been put into the development of solid-state electrolytes. A typical solid-state electrolyte consists of a polymer membrane, such as polyethylene oxide, complexed with an alkali metal salt [73,77]. While the solid polymer electrolytes are indeed safer compared to liquid electrolytes due to their dimensional stability and prevented Li dendrite growth, their ionic conductivity is poor, and this limits their application [74,78,79]. Solid-state electrolytes can also consist of inorganic materials that conduct ions by diffusion through the lattice. They have high ionic conductivities and good mechanical properties but are also brittle and poorly compatible with the electrode surface [80]. A compromise between the solid-state and liquid electrolyte is a gel electrolyte. It is obtained by swelling the polymer membrane with an electrolyte solution [81,82]. They are an attractive option due to their low volatility, high thermal stability, reduced packaging size and safety. The electrochemical performance of the gel electrolytes is determined by the liquid used in the swelling and the mechanical and safety properties by the polymer matrix [81].

There are several other types of electrolytes as well, and of these ionic liquids are probably the most investigated. Ionic liquids are ionic compounds that have a melting point below 100 °C [73,83]. The vapor pressure of ionic liquids is negligible which means that they are inflammable. Combined with the large electrochemical stability window, they are considered a very safe option for liquid electrolytes [84]. However, they are

also more expensive and very viscous, making them difficult to handle compared to liquid electrolytes.

2.4 Other materials in Li-ion battery

In addition to the active material, an electrode in Li-ion battery contains a few other components, such as conductive and binding materials mixed with the active material, the whole mix then coated on a current collector. The conductive component is used to enhance the often-insufficient conductivity of the active electrode materials. The most used conductor material is carbon black [85], but new alternatives such as CNTs [86] and poly(3,4-ethylenedioxythiophene)-poly(styrenesulfonate) [87,88] have recently gained interest as well.

Binders, on the other hand, attach the active material to the current collector. The binder materials are typically polymers, with polyvinylidene fluoride (PVDF) one of the most used ones due to its good electrochemical stability, binding capability and ability to absorb electrolyte to enable Li-ion transportation to the active material surface [89,90]. However, to dissolve PVDF, toxic and environmentally unfriendly N-methyl-2-pyrrolidone (NMP) has to be used as a solvent [91]. In addition, PVDF has been reported to not withstand the large volume changes occurring in some negative electrode materials such as Si [92]. Because of this, alternative materials have been investigated actively, and the promising materials include polymers such as carboxymethylcellulose (CMC)-based binders [93–95], polyacrylic acid (PAA) [92,96] and styrene butadiene (SBR) [97].

To dissolve the binder and to form a paste that can be applied on the current collector, the electrode material and additives are mixed in a solvent. NMP is one of the most used ones due to wide use of PVDF, but it is, as already mentioned, harmful for environment and also quite laborious and expensive to use [98]. Because of this, replacements for NMP are being searched actively, water being the top alternative. Advantages of water include e.g. low cost, environmental-friendliness and fast drying speed after electrode coating. Several already used binders, such as CMC and SBR, are also water compatible [99].

Current collectors in Li-ion batteries are usually metal foils, Al foil for positive electrode and Cu foil for negative electrode. If the negative electrode active material has a voltage window that does not go below the Li-Al alloy formation potential, Al is used on the negative electrode as well because it is cheaper.

A final material group discussed in this work is the separator materials. Separator plays an important part in Li-ion battery by physically separating the electrodes but permitting Li ions dissolved in the electrolyte to freely flow through them from electrode to electrode. Porous polymer membranes are the most popular, with most of the commercially available ones made of e.g. polypropylene (PP), polyethylene (PE), or other polyolefins [100]. However, the thermal stability of polymer membranes is typically quite low and to improve the safety of the battery cells, alternative materials have been developed. These include for example, nonwoven fabrics made of polymers such as PVDF, PE or polyacrylonitrile [101–103], and ceramic separators made of e.g. Al_2O_3, SiO_2 and MgO [104]. Composites using material from more than one group are also usual [105].

3. Experimental methods

3.1 Structural characterization

The structure and morphology often considerably affect the performance of the electrode materials. They can be investigated with several different material characterization methods with the observed properties depending on the method used. In this thesis, scanning electron microscopy (SEM), transmission electron microscopy (TEM), inductively coupled plasma optical emission spectroscopy (ICP-OES), atomic absorption spectroscopy (AAS), X-ray diffraction (XRD), X-ray photoelectron spectroscopy (XPS), X-ray absorption near edge spectroscopy (XANES), electron energy loss spectroscopy (EELS) and Raman spectroscopy were used.

SEM is an electron microscopy technique used to image sample surfaces using an electron beam [106]. It was utilized in all Publications to observe the size and morphology of the investigated materials. In addition, the changes induced by material aging, such as cracking, were investigated with SEM in Publication IV. TEM is an electron microscopy method like SEM. However, instead of scanning the sample with the electron beam as is done in SEM, in TEM the beam is transmitted through the sample. TEM has higher resolution than SEM, and with it even the atomic level structure of materials can be investigated. [107] In this thesis, TEM was mostly used together with EELS.

ICP-OES and AAS are tools to investigate the elemental composition of materials. In this thesis, ICP-OES was used to determine the composition of synthetized positive electrode materials (Publications I-IV). AAS was used to compare the composition of fresh and aged electrodes in Li-ion batteries (Publication IV). While the elemental composition can be determined well with ICP-OES and AAS, they cannot detect the chemical composition or the valence states of the elements. Because of this, XANES and EELS were used to obtain information about the chemical environment of the elements. XANES is an underclass of X-ray absorption spectroscopy (XAS), which is an element specific method to probe the local electronic and geometric structure around atoms or ions absorbing a X-ray photon [108]. XANES can give information on the oxidation state and the local symmetry around the absorbing ion or atom. For a long time XAS (and XANES) measurements were available nearly exclusively at synchrotrons. During recent years however, the improvements in X-ray crystal optics have enabled the XANES measurements in laboratory scale using conventional X-ray tubes [109–113]. EELS is a spectroscopy method used in TEM, and in the method, the investigated material is exposed to an electron beam with a known range of kinetic energy. The electrons interact with the material and part of them scatters and loses energy that can be measured [114]. EELS is an element and valence state specific

method. Laboratory-scale XANES was used in Publication I to determine the changes in Co valence upon aging, and EELS in Publications I, II and IV to investigate the effect of phase impurities on the Co and O valence states.

XRD is a standard tool to study the bulk crystalline structure of the materials. In the technique, a sample is exposed to X-rays which interact with the sample producing constructive interference if Bragg's law ($n\lambda = 2d{\cdot}\sin\theta$) is fulfilled. By scanning the sample through a range of 2θ directions, a phase-specific diffraction pattern can be obtained [115,116]. In Publications I-IV, XRD was used to determine the crystalline structure and the phase impurities in the investigated materials. In addition, in Publication IV it was used to determine the structural changes induced by aging and re-lithiation.

The chemical composition in the particle surface and its vicinity can be investigated with Raman spectroscopy and XPS. Raman spectroscopy is a technique used to measure molecule vibration modes. The sample is exposed to a laser of visible, near-ultraviolet or near-infrared light which interacts with the material. As a result the energy of some of the light photons is shifted, and the change can be measured. [117] The penetration depth for Raman spectroscopy using green laser is 50–100 nm [118]. In XPS, the measured sample is excited using X-rays, which causes it to emit photoelectrons. The energy of the emitted photoelectrons is measured to form a spectrum that can be used to identify the elemental composition of the sample, as well as the chemical state of the elements. [119] The penetration depth for XPS is approximately 10 atoms layers, making it ideal for observing the surface composition. XPS can also detect Li directly, which gives it a large advantage in the investigation of Li-ion battery chemicals. Raman spectroscopy was used in Publications I, II and IV to investigate the chemical state on the outer part of $LiCoO_2$ particles. In addition, it was also used to investigate the structural changes in the material induced by aging in Publication IV. XPS was used in Publication I to observe the differences in the Mg and Li distributions in the differently doped $LiCoO_2$ particles.

3.2 Electrode and cell preparation

The electrodes for electrochemical tests used in this thesis were prepared by mixing the active material with conductive carbon and PVDF as a binder. NMP was used as a solvent to form a slurry which was coated on a metal foil (Al for positive electrodes, Cu for negative electrodes) using doctor blade coating technique. The consistency of the slurry, the coating thickness and the calendaring pressure were optimized for desired electrode loading and the best electrochemical performance. The electrodes were cut and then dried under vacuum (≥110 °C) overnight before transferring into a glovebox (Ar) to be assembled to test cells.

In Publication IV, the reuse of aged positive electrode materials was investigated. For this purpose, aged electrodes were collected from pouch cells. The cells were opened in the glovebox and the components separated. After this the positive electrodes were rinsed, dried, and cut before assembling to the new test cells.

The electrochemical characterization of the materials was carried out in three different types of cells: half-cells, full-cells, and three-electrode cells. In half-cells the investigated material is used as a working electrode and metallic Li as a counter electrode. The half-cells are useful when only one material is investigated, and they are simple and easy to use. However, the standard organic electrolytes used in the cells

are not stable on Li surface, which leads to the formation of a SEI layer [120]. The SEI layer thickens upon cycling, which leads to increase in impedance and in the worst case to electrolyte drying. In addition, the excess amount of Li provided by the Li counter electrode can hide the Li loss in the investigated electrode. Therefore, it is important to test the materials in full-cell set-ups as well, especially if the measurement is long. In full cells, both electrodes are Li insertion compounds with different reaction potentials. In this thesis, the investigated materials were used as positive electrodes and graphite as a negative electrode. As the electrochemical system was packed in a laminated Al pouch, the full cells used in this work are called pouch cells.

Similarly to half-cells, in three-electrode cells the investigated material is used as the working electrode and Li as the counter electrode, but in addition a reference electrode is added. In this thesis, metallic Li was used. As the potential of the counter electrode changes slightly when current is applied to the cell, the use of a separate reference electrode enables the exact determination of the potential of the investigated material in the working electrode. The risks related to Li counter electrode are present in three-electrode cells as well, but the system, contrary to half-cells, often enables the use of excess electrolyte which decreases the risk of the electrolyte drying. Li ions containing organic electrolyte was used in all cell types, the most used being 1 M $LiPF_6$ in 1:1 EC:DMC solution.

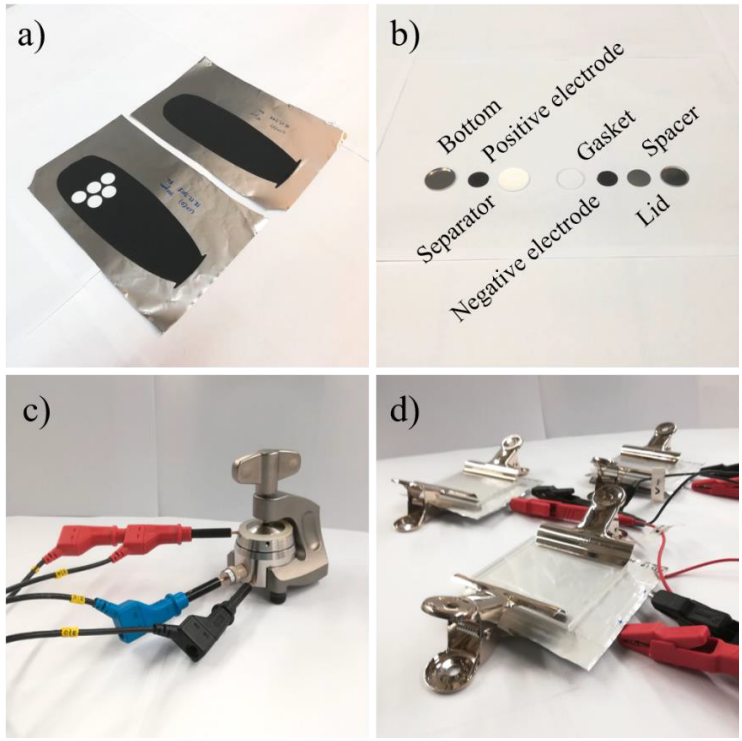

Figure 4. Li-ion battery cell preparation in this thesis. a) Slurries coated on Al foil with doctor blade technique, b) coin cell parts in order of assembly, c) three-electrode cell setup, d) pouch-cell setup.

3.3 Electrochemical characterization

The electrochemical characterization methods used in this thesis are galvanostatic charging and discharging i.e. cycling, galvanostatic intermittent titration technique (GITT), cyclic voltammetry (CV) and electrochemical impedance spectroscopy (EIS). The most used of these is galvanostatic cycling that is used to test how the investigated material responds to continuous charging and discharging. In this method, a constant current is applied to the cell and the response in voltage is recorded until a set cut-off voltage or time is reached. By changing the measurement parameters, different properties of the material can be investigated. In rate capability measurement, the charging and discharging are done using several different currents and cell capacity is calculated. This gives information on how the investigated material responds to high current. If, on the other hand, the material durability is tested, the number of charge-discharge cycles is increased, and the capacity retention of the material is monitored. The galvanostatic measurements are generally done in half-cells if the material properties are tested. If the material is already proved to perform well, cycling might be done in pouch cells to test the behavior of the material in a more realistic environment. In this thesis, long-term pouch cell cycling was performed in Publications I and II.

In CV measurements, the voltage is linearly scanned between two pre-determined values and the current response is recorded. The obtained data gives information about the electrochemistry of the cell, for example occurring reactions and their kinetics. [121] The technique was used in all Publications in this thesis.

GITT is a method to investigate the kinetic and thermodynamic parameters of a material [122]. In Publication II the method was used to determine the diffusion coefficients of the investigated materials. In the measurement, similarly to galvanostatic cycling, a constant current pulse is applied to the cell. However, the pulses used in GITT are short and are followed by a relaxation time, during which no current passes through the cell. At the end of the relaxation time the cell voltage is recorded, and the next pulse is applied. The pulses are continued until the pre-determined voltage limit is reached. [122,123] By plotting the relaxation time voltage against the titration step and the voltage during the current pulses against the current pulse duration, the diffusion coefficient of the material can be calculated followingly:

$$D = \frac{4}{\pi}\left(\frac{iV_m}{z_A FS}\right)^2 \left[\frac{\left(\frac{dU}{d\delta}\right)}{\left(\frac{dU}{d\sqrt{t}}\right)}\right]^2 \quad t \ll \frac{l^2}{D} \qquad (1)$$

where i is the current, V_m is the molar volume of the active material, z_A is the charge number, F is the Faraday's constant, S is the electrode/electrolyte contact area and l is the diffusion length, e.g. the particle radius. $dU/d\delta$ is the slope of the relaxation time plotted against the titration step, i.e. the stoichiometry of the inserted atoms. $dU/d\sqrt{t}$ corresponds to the slope of electrode potential during the current pulse plotted against the square root of time.

EIS is a technique used to determine the internal resistance of the cell, which is affected by e.g. temperature changes or aging. In the technique a sinusoidal signal is applied to the cell and the response is recorded as a function of frequency. The applied signal can be a potential or a current signal and the response is the other. I.e., if a potential signal is applied, the response signal is a current signal. [124] The data is often

presented in Nyquist plane plots, in which the real part of the cell impedance is presented in horizontal axis and the complex part in the vertical axis. Based on the plot, several processes such as ionic and electronic conduction, charge transfer and mass transfer can be investigated. The EIS measurements in this work were performed in three-electrode cells, as the impedance of the Li counter electrode used in half-cells is large and unstable. In addition, in Publications I and II the impedance of the pouch cells was measured.

4. Doping of layered transition metal oxides

Doping is one of the most used methods to improve the electrochemical performance of layered transition metal oxides. In this chapter, the effect of doping, along with a few other modification methods, on the electrochemical performance of layered transition metal oxides is discussed. The chapter focuses especially on understanding the effect of the synthesis step in which the dopant is added and on comparing dual doping to Li doping. $LiCoO_2$ is used as an example material, as it is a well-established material in the literature, and has a similar but simpler structure than most of the other layered transition metal oxides.

4.1 Factors affecting the performance of layered transition metal oxides

Layered transition metal oxides ($LiMO_2$, M = Co, Ni, Mn etc.) are the most used materials in Li-ion battery positive electrode [21]. During the last three decades, the materials have been intensively researched to optimize their electrochemical performance and stability. The typical modifications to improve the material performance include particle size and morphology changes [125,126], coating [127,128], chemical gradient composition [129,130], Li/transition metal stoichiometry [131,132] and doping [125,133], with most of the variations obtained through changes in the synthesis processes. One of the most common synthesis processes and the one used in this work is solid-state method, in which the precursors are mixed and heated at high temperature to form the synthesized compound [134–137]. Other common methods include e.g. sol-gel [138,139], co-precipitation [140–142], and hydrothermal [143,144] processes.

Particle size and morphology are one of the most important factors affecting the electrochemical performance of positive electrode materials. Generally, it can be said that the smaller the particle size is, the better the rate capability of the material becomes due to shortened diffusion distances for Li ions [139,143]. However, with decreasing particle size the surface area increases, and this exposes the material more to irreversible structure changes occurring in the surface, which leads to faster degradation during long-term cycling [143]. Morphology affects the electrochemical performance similarly, particles with large surface area having a high rate capability while the capability of the low-area materials is poorer [144,145]. Depending on the material application, the particle size and morphology are optimized to match the requirements.

In addition to particle size and morphology, the electrochemical properties of the layered transition metal oxides can be modified through changes in the chemical state. As most of the side reactions occur on the particle surface, coatings and gradient compositions are effective blocking them away and improving the capacity retention [127–129,133]. However, the synthesis of coatings and gradient compositions is often complicated compared to simple synthesis process of layered transition metal oxides, and this restricts their use.

The stoichiometry of the layered transition metal oxide affects its electrochemical performance as well. Due to SEI layer formation in the Li-ion battery negative electrode, part of the cyclable Li in the positive electrode is lost already during the first few cycles [146]. To compensate the Li loss, the positive electrode material can be synthesized with over-stoichiometric Li/Co ratio > 1. In Li-rich LCO for example, the excess Li replaces some of the Co and the charge deficit is compensated with oxygen vacancies [131] or oxidation of Co^{3+} to Co^{4+} [147]. The Li excess has been shown to suppress phase transitions occurring during the cycling and to increase the conductivity. However, upon cycling the capacity retention of the Li-rich LCO is poorer than stoichiometric LCO's due to its gradually decreasing voltage profile which reaches the cut-off voltage sooner [131].

In doping, a small amount of additional compound or element is mixed to the host material. The process is easy, as the addition can be done simultaneously in the synthesis with Li and Co precursors, but already a small amount of dopant may have a large effect on the electrochemical performance of the material. Because of these reasons, doping is one of the most popular methods to enhance the electrochemical performance of layered transition metal oxides. Layered transition metal oxides are typically doped with cations such as Al^{3+} [148–150], Mg^{2+} [150–156], Ti^{4+} [157,158] and Zr^{4+} [159,160]. In addition, with the use of recycled battery chemicals being in a rise, impurities such as Cu can also be found from the layered transition metal oxides [161,162], and they can be considered as dopants as well. The changes induced in the transition metal oxide depend on the dopant and typically include enhancements such as crystal structure stabilization [150–152,163,164], reduced positive electrode dissolution [125,165], enhanced conductivity [125,160,166,167] and enhanced Li diffusion through changes in the crystal structure [163,168,169] and morphology [148,170].

Layered transition metal oxides, such as $LiCoO_2$, have a layered $R\bar{3}m$ structure that consists of alternating transition metal oxide (e.g. CoO_2) and Li layers [2]. When a cationic dopant is added to the structure, it replaces either Li or the transition metal, depending on the valence and size of the dopant [171]. Divalent dopants, such as Mg, can occupy both Li and transition metal sites, the occupancy of the dopants depending mostly on the synthesis temperature with the higher temperature increasing the amount of dopant on the transition metal site [164]. The trivalent and tetravalent dopants generally occupy the transition metal site increasing the lattice spacing and decreasing the band gap [171]. The downside of using electrochemically inactive dopants is that they replace active cations and thus reduce the capacity.

Addition of dopants with valences differing from valence of the transition metal oxide induces changes in the electronic structure of the elements. In LCO, if a tetravalent dopant is added on Co^{3+} site, the charge is compensated through formation of Co^{2+} [172]. If a divalent dopant is added, a corresponding amount of Co^{3+} will turn to Co^{4+} or alternatively, an oxygen deficiency is formed to preserve the charge balance [173]. Changes in the electronic structure can enhance the electric conductivity of the

doped material, which leads to better electrochemical performance. E.g., addition of Mg^{2+} in the LCO Co site has been reported to enhance the electronic conductivity [153,173,174]. However, the change in Co valence leads to a loss of electrochemically active cations [152]. Considering that the electrochemically inactive dopants already replace the active cations and thus reduce the capacity, this increases the capacity drop further. An approach to stabilize the charge deficit is the insertion of two dopants, one tetravalent and another divalent [152,175]. In this case the valences of the cations cancel each other, and electrochemically active Co^{3+} is not lost. This dual doping is interesting also because in the optimal case, the pros of two dopants can be combined even if the valences of the dopants do not cancel each other. Recently, the dual doping has gained interest in the literature, the investigated pairs including e.g. Ba & Ti [176], Mg & Mn [152], Mg & Zr [160], Mg & Ti [169,175] and Al & Ti [177,178].

4.2 Effect of adding dopant at different synthesis stages

While the use of different dopants in different concentrations have been investigated in several layered transition metal oxide materials, adding dopant to the precursor before the final solid-state synthesis of the transition metal oxide has been ignored in the literature. Simultaneously, with increasing Li-ion battery consumption, the need for raw materials is increasing. Using recycled layered transition metal oxides is a logical way to increase the raw material supply and there have already been several studies reporting the performance of recycled positive electrode materials [161,179–181]. However, the active material is often mixed with the other cell components in the current recycling techniques [182–184], which leads to impurities in the regenerated product [161,185]. The impurities affect the electrochemical performance of the material, and understanding the effects is important.

In Publication I, precursor-doping of LCO was compared to a conventional doping method done during the final synthesis in LCO, also called lithiation. Mg was selected as a dopant because its use in LCO and other transition metal oxides is quite established, and it is known to enhance the structural stability and conductivity of LCO in small amounts [152]. The effect of the doping step was compared in two Li/Co ratios as well, to understand whether the doping is dependent on the material stoichiometry. The materials were synthesized using the same solid-state synthesis process to ensure the comparability. Description of the preparation of the differently doped LCOs is presented in Figure 5.

The composition of the samples was measured with ICP-OES, and the measurements show that the doped samples contain 0.5–0.6 mol-% of Mg, and that the stoichiometrically synthesized samples have the Li/Co ratios of 1.01, 1.03 and 1.02 for non-doped (s-LCO), lithiation doped (s-L-LCO) and precursor doped (s-P-LCO), respectively, while the Li-rich samples have the Li/Co ratios of 1.04, 1.05 and 1.04 for non-doped (o-LCO), lithiation doped (o-L-LCO) and precursor doped (o-P-LCO) samples, respectively. The SEM measurements (Figure 6) show that the lithiation doping decreases the primary particle size in the particle surfaces, the lithiation-step doping inducing lattice distortions in the material, which leads to the robust morphology.

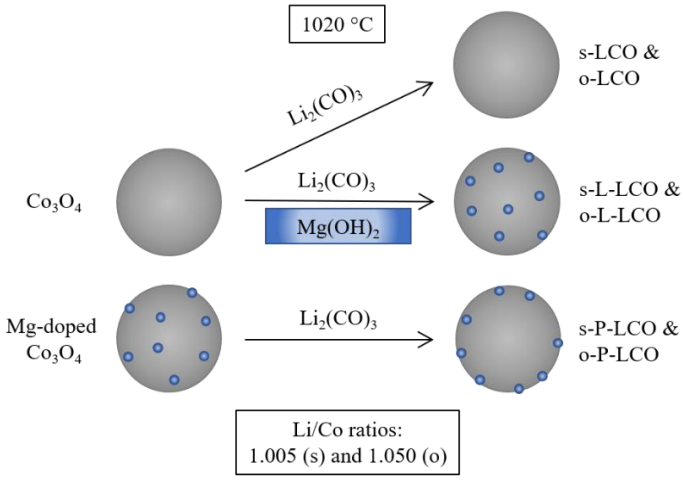

Figure 5. Synthesis process of the Mg-doped LCOs synthesized in different doping stages.

In the electrochemical characterization, the doping step is found to affect the electrochemical performance of Mg-doped LCO. The cyclic voltammograms of the materials are presented in Figure 7 and three peaks typical for $LiCoO_2$ can be observed during both the Li insertion and extraction scans for all the materials. The largest peak pair at 3.9 V vs. Li^+/Li is related to the Li de-intercalation/intercalation reaction during two-phase insulator-metal transition [16,186], while the peaks at 4.05 V vs. Li^+/Li and 4.20 V vs. Li^+/Li are related to Li order-disorder transitions at $x = 0.5$ in Li_xCoO_2. The peak separation is observed to be larger for the precursor-doped LCO than for lithiation-doped LCO in both stoichiometric and Li-rich Li/Co ratios indicating that the electrode reaction for the precursor-doped sample is more irreversible. In non-doped and precursor-doped LCOs the Li excess is observed to decrease the reversibility, but in lithiation-doped LCO the Li excess increases it slightly, which is attributed to even distribution of Mg in the sample reducing the lattice distortions induced by Li over-stoichiometry.

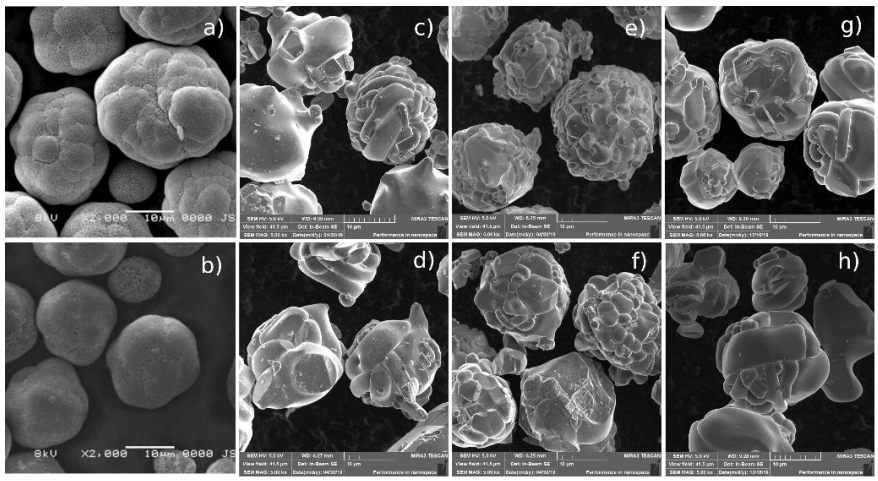

Figure 6. SEM images of the a) Co_3O_4 precursor, b) Mg-doped Co_3O_4 precursor, c) s-LCO, d) o-LCO, e) s-L-LCO, f) o-L-LCO, g) s-P-LCO, h) o-P-LCO powders. The scale bar length is 10 µm.

The peak intensity is also observed to vary between the samples, which indicates that there are differences in the electrode kinetics. The peaks for lithiation-doped samples are sharper than for the precursor-doped samples, which suggests that the precursor doping increases the resistance of the LCO compared to the lithiation doping. The doping step affects the reversible capacity of LCO as well. In voltage range of 3.0–4.4 V the o-LCO and o-L-LCO show the highest charge capacities, 178.3 mAh g^{-1} and 177.7 mAh g^{-1}, respectively. The high capacity of these materials is attributed to the excess lithium, whereas the slightly lower capacity of the o-L-LCO compared to o-LCO is ascribed to the electrochemically inactive Mg doping. These two LCOs are followed by s-LCO and s-L-LCO with the charge capacities of 176.5 mAh g^{-1} and 174.0 mAh g^{-1}, respectively. Similarly to the Li-rich samples, the slightly decreased capacity of the s-L-LCO is attributed to the Mg doping. Interestingly, the precursor doped LCOs have the lowest charge capacities, being 172.4 mAh g^{-1} and 170.7 mAh g^{-1}, respectively. The smaller capacities compared to the lithiation-doped samples are attributed to the larger primary particle size on the particle surfaces.

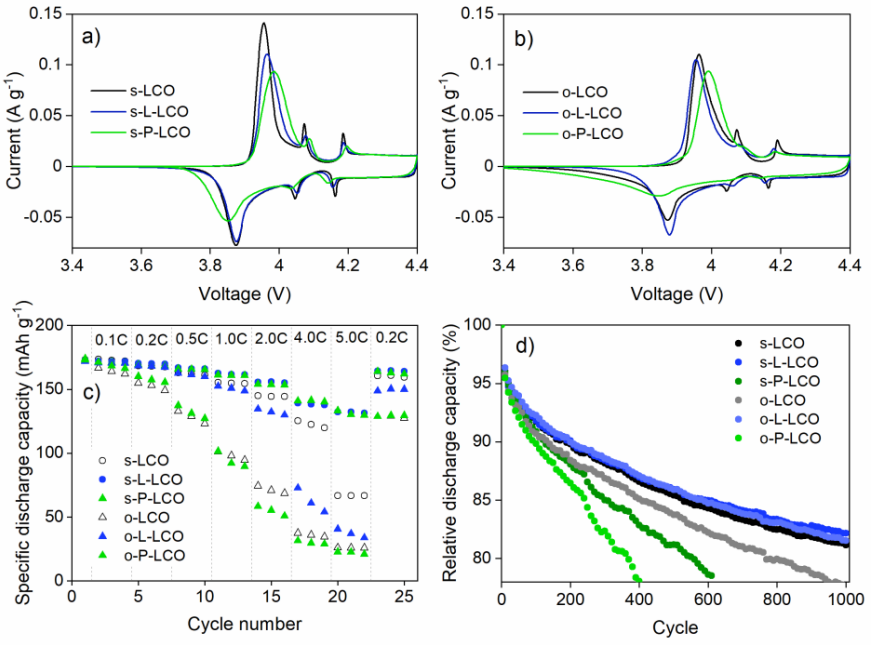

Figure 7. Electrochemical performance of the LCO materials synthesized using different doping stages. a) Cyclic voltammograms of the samples with the stoichiometric Li/Co ratio at scan rate of 0.02 mV s^{-1}, b) Cyclic voltammograms of the samples with the Li-rich Li/Co ratio at scan rate of 0.02 mV s^{-1}, c) rate capability, d) long-term cycling of LCO/graphite pouch cells cycled using C-rate of 0.5 C. Cyclic voltammograms and rate capability are measured in half-cells using the voltage range of 3.0–4.4 V and long-term cycling in pouch cells using the voltage range of 3.0–4.3 V.

The long-term cyclability of the differently doped LCOs was investigated by cycling them in LCO/graphite pouch cells in the voltage range of 3.0–4.3 V (Figure 7d). The lithiation-doped samples are observed to perform well, reaching 1000 cycles at the SOH of 82 %. The precursor-doped samples, however, have a poorer capacity retention, reaching SOH 80 % already after 550 (s-P-LCO) and 350 (o-P-LCO) cycles. Of the non-doped samples, s-LCO has similar capacity retention to the lithiation-

doped LCOs while the o-LCO has slightly poorer capacity retention, reaching SOH 80 % at 800 cycles. When the lithiation-doped samples are compared to the non-doped samples, the lithiation doping is observed to enhance especially the performance of the Li-rich samples. The precursor doping, on the other hand, worsens the cyclability of the LCO regardless of the Li/Co ratio, and compared to the lithiation-doped LCO, the performance is especially poor.

To understand the differences in the cyclability of the differently doped LCOs, EIS measurements were conducted, and the results are presented in Figure 8. All the spectra have a similar shape, consisting of three semicircles and a diffusion tail at low frequency. The first high-frequency semicircle is attributed to the active material/current collector interface resistance, and no notable differences between the materials are observed. The second semicircle at mid-frequencies corresponds to the charge-transfer resistance of negative graphite electrode and it overlaps strongly with the third semicircle attributed to the charge-transfer resistance of the positive LCO electrode. The sum of the charge-transfer resistances in the pouch cells agree with the three-electrode measurements of the LCO materials, and based on this, the differences in size are concluded to be caused by the changes in the LCOs.

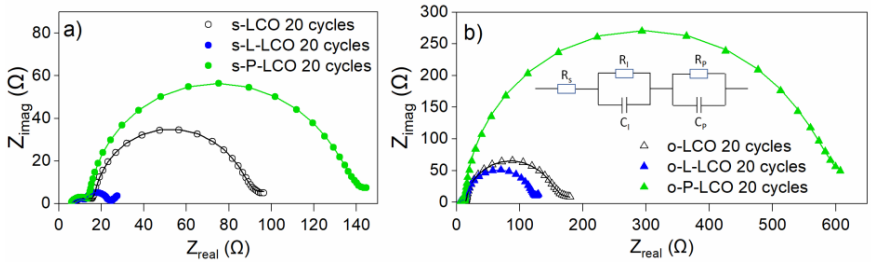

Figure 8. Nyquist diagrams of the investigated LCOs in LCO/graphite pouch cells at SoC of 50 % cycled in the voltage range of 3.0–4.3 V. a) stoichiometric LCOs after cycling, b) Li-rich LCOs after cycling. Experimental data is presented as dots and fitted data based on equivalent circuit as lines.

The pouch cells are observed to have differences already at the beginning of the cycling. Generally, the lithiation-doped samples have slightly smaller charge-transfer resistances than the non-doped ones, while the precursor-doped samples have larger. The initial charge-transfer resistance of s-P-LCO is especially large, which is attributed to the Co_3O_4 layer observed at the particle surface in Raman spectroscopy. After the cycling, the charge-transfer resistances can be observed to have increased. The increase is largest for the precursor-doped LCOs and smallest for the lithiation-doped LCOs, which is in agreement with the capacity retention data, the high charge-transfer resistance leading to poorer cyclability. The results indicate that lithiation-step Mg doping successfully reduces the increase of the charge-transfer resistance during cycling in both stoichiometric and Li-rich LCO. The precursor doping on the other hand, increases the charge-transfer resistance. The better cycle life and smaller charge-transfer resistance of the lithiation-doped LCOs is attributed to several factors. First, the stacking order is slightly better for the lithiation-doped samples, especially compared to the precursor-doped LCOs, which might have enhanced the stability of the lattice upon long-term cycling. Second, the XPS measurements show that Mg is distributed in the lattice of the lithiation-doped LCOs more evenly than in the precursor-doped LCOs in which Mg is concentrated on the particle surfaces. The high Mg concentration on the surface might increase the amount of electrochemically

inactive Co and thus hinder the charge transfer. Finally, the XANES investigations show that the reachable Co valence decreases as the materials age. The decrease is smaller for the lithiation-doped LCOs than for the precursor-doped, which indicates that it reflects the material aging and can perhaps be used as an indicator of the cell health in the upcoming investigations.

As a conclusion, the doping-step has a clear effect on the performance of $LiCoO_2$. The doping is found to enhance the even distribution of the dopant in the sample, which in turn improves the cyclability of the material. The effect of doping on the rate capability is smaller, and in stoichiometric samples, there are no differences between lithiation and precursor doping. It is therefore concluded that the long-term measurements are necessary to fully understand the effect of the doping step on the material performance. In addition, the results indicate that even generally advantageous dopants cannot be left in the material as impurities during material recycling, as they might have surprisingly large effect on the material performance.

4.3 Comparison of dual doping and Li excess

In Publication II, the performance of Mg and Ti dual-doped LCO was compared to stoichiometric and Li-rich LCO. This was investigated to understand how the different doping approaches (dual doping vs Li doping) work in relation to each other and how they affect the electrochemical performance, especially the cyclability, of LCO. The materials were synthesized using the same solid-state synthesis method to ensure the comparability of the samples. The Li/Co ratios were determined with ICP-OES to be 0.97, 1.00 and 0.98 for the stoichiometric (LCO(S)), Li-rich (LCO(R)) and Mg-Ti-doped (LCO(D)) LCOs, respectively, and the dopant concentrations for LCO(D) to be 0.46 mol% and 0.18 mol% for Mg and Ti, respectively.

The electrochemical performance of the materials was investigated with CV using scan rates of 0.02 mV s^{-1} and 0.05 mV s^{-1}. The voltammograms are presented in Figure 9 and they show the typical three phase-transitions of $LiCoO_2$, a two-phase semi-conducting/metallic transition at 3.9 V, and Li ordering transitions at 4.05 and 4.20 V. The intensities of the Li insertion peak vary, the intensity of the LCO(D) being much higher compared to the LCO(S) and LCO(R), which indicates smaller resistance for the Mg-Ti doped sample. At the higher scan rate of 0.05 mV s^{-1}, the Li insertion peak positions of LCO(S) and LCO(R) are observed to shift to lower voltages, which indicates that the overpotential of these samples is larger compared to the LCO(D). The high overpotential of the two samples is attributed to increasing resistance caused by structural deterioration and electrolyte oxidation on the sample surfaces. The Li excess is concluded to worsen the effect while Mg-Ti doping is shown to prevent these changes.

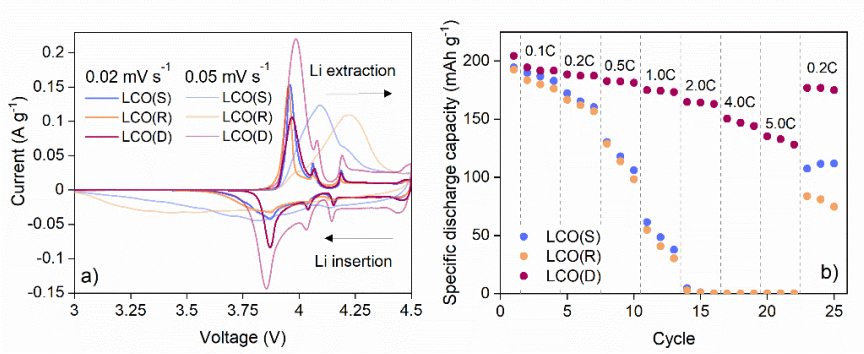

Figure 9. a) Cyclic voltammograms of the stoichiometric, Li-rich and Mg-Ti-doped LCOs in half-cells using scan rates of 0.02 mV s^{-1} (solid lines) and 0.05 mV s^{-1} (dashed lines) in the voltage range of 3.0–4.5 V, b) rate capability of the stoichiometric, Li-rich and Mg-Ti-doped LCOs in the voltage range of 3.0–4.5 V.

Rate capability measurements were performed to investigate the electrochemical performance of the LCO samples at higher currents (Figure 9b). A commercially interesting voltage range of 3.0–4.5 V was used as it represents the widest range LCO can be cycled with acceptable cycle life [152]. The average initial discharge capacity of LCO(D) is 204 mAh g^{-1} while for LCO(S) and LCO(R) it is 195 mAh g^{-1} and 193 mAh g^{-1}, respectively. At high currents, the difference between LCO(D) and the other two increases, and at 5C the LCO(D) discharge capacity is 135 mAh g^{-1} while for LCO(S) and LCO(R) it is 0 mAh g^{-1}. The better rate capability of LCO(D) is attributed to better electronic and ionic conductivity determined with EELS and GITT. First, EELS results show that the Co valence in the LCO powders is slightly lower in LCO(D) compared to the others. This is attributed to the partial reduction of Co^{3+} to Co^{2+} upon Ti^{4+} doping which increases the number of charge carriers and thus leads to higher electronic conductivity. Mg is determined to occupy both Li and Co sites in the lattice structure, thus not affecting the Co valence state. The ionic conductivity was investigated with GITT and the results show the Li diffusion coefficient to be highest for LCO(D) indicating the highest ionic conductivity. This is explained by the SEM images which show that the primary particle size of LCO(D) is smaller compared to the LCO(S) and LCO(R). The smaller particle size decreases the Li diffusion distance and thus enhances the ionic diffusion.

The long-term stability of the stoichiometric, Li-rich and Mg-Ti-doped LCOs was investigated in pouch cells using graphite as a negative electrode. The cycling in high voltage range of 3.0–4.4 V is compared to the traditional voltage range of 3.0–4.2 V, and the results are presented in Figure 10. The capacity retention for LCO(D) cells is clearly the best in both the voltage ranges, being 89 % after 1000 cycles in the lower voltage range and reaching 240 cycles in the higher voltage range. Based on the rate capability measurements, the good performance of LCO(D) was expected. The other two materials, however, did not perform as well. In the lower voltage range, the capacity retention of the LCO(S) cells is clearly better than that of the LCO(R) cells. This is surprising, because based on the half-cell tests (Figure 9), LCO(S) was expected to have similar cycle life to LCO(R). While this could not be fully explained, the difference is attributed to the different electrolytes used in the half-cells (1 M $LiFP_6$ in 1:1 EC:DMC) and in the pouch cells (1 M $LiPF_6$ in 25:70:5 EC:DEC:PC with 1 mol% VC and 1 mol% PS), as the electrolyte can affect the material cyclability. In the larger

voltage range, LCO(S) and LCO(R) show both poor capacity retention, reaching 80 % already after 50 cycles. Below 80 % the performance of LCO(R) is slightly better, indicating that the excess Li enhances the performance in high voltage range.

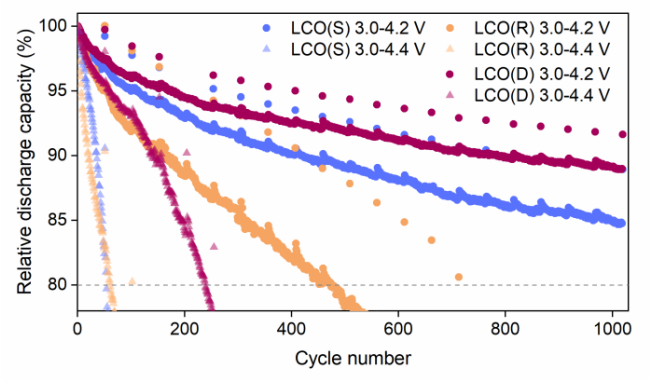

Figure 10. Relative capacity drop of the LCO/graphite pouch cells cycled with C-rate of 0.5 C.

EIS spectra were measured to investigate the changes in internal resistances of the LCO materials induced by the cycling. The impedance data of the LCO/graphite full cells before and after cycling presented in Figure 11 consists of two semicircles and a straight or slightly curved line. The smaller one of the semicircles observed at high frequencies is attributed to the SEI on the graphite electrode. The larger semicircle at mid-frequencies corresponds to the charge-transfer resistances of both the positive and negative electrode. Both electrodes typically generate their own semicircles, but the electrode processes occur at close frequencies, which leads to the semicircles overlapping. While the overlapping electrodes makes identifying in which electrode the changes occur difficult, most of the differences are presumed to be caused by the positive electrode because a similar negative electrode is used in all cells. The line at low frequencies originates from solid-phase Li diffusion.

The sizes of both the high-frequency and the mid-frequency semicircles are observed to increase upon cycling. The increase in the high frequency semicircle indicates thickening of SEI layer caused by slow electrolyte decomposition at the graphite electrode. The increase of the mid-frequency semicircle indicates the increase of the charge-transfer resistance in the electrodes. In the low voltage range, the increase is the fastest for LCO(R) cells while the slowest for LCO(D) cells. In the high voltage range the increase is the fastest for LCO(S) while the slowest for LCO(D) cells, which is in agreement with the cycling results, the longest cycle life matching the smallest increase in charge-transfer resistance. As the charge-transfer resistance of the LCO(D) increases the slowest, the doping can be concluded to stabilize the LCO structure in both voltage ranges, slowing the material degradation. The large charge-transfer resistance of LCO(R) cells is explained by the poorer crystallinity of the sample, the Li excess inducing slight disordering in the sample.

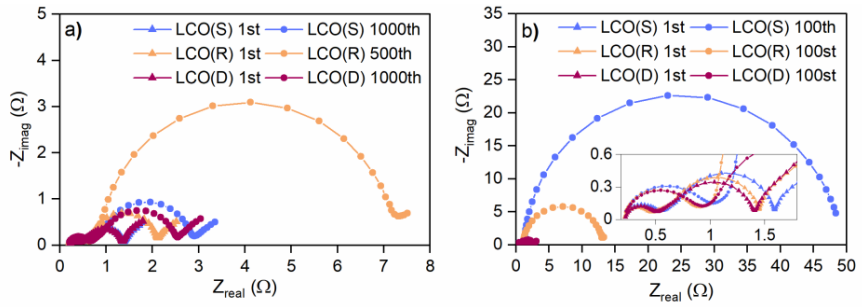

Figure 11. Nyquist diagrams of LCO-graphite pouch cells at the beginning of cycling and at the end of cycling with C-rate of 0.5C in the voltage ranges of a) 3.0–4.2 V and b) 3.0–4.4 V.

To conclude, Mg-Ti dual-doping is observed to have a positive effect on enhancing both the rate capability and cycle life LCO. Li excess on the other hand is observed to deteriorate the electrochemical performance. The results indicate that certain additives can have a large benefitting effect on the material performance, but the added elements should be selected carefully. The dual doping is shown to successfully improve the cycle life of LCO, and this could be utilized in improving the sustainability of the layered transition metal oxides.

4.4 Remarks on the lithiation doping of LCO

In both Publications I and II, lithiation doping was observed to improve the performance of LCO, Mg doping in Publication I and Mg-Ti doping in Publication II. The materials were investigated using different voltage ranges, and therefore, direct comparison between the materials cannot be done. However, there are similarities and differences in the material behaviors, and they are discussed here briefly.

First, the Mg doping and the Mg-Ti doping affect the initial discharge capacity differently. The Mg doping decreases it slightly, the initial capacity of Mg-doped LCO being 174.0 mAh g^{-1} while the capacity of non-doped LCO is 176.5 mAh g^{-1}. On the other hand, the initial capacities of Mg-Ti-doped and non-doped LCOs are 204 mAh g^{-1} and 195 mAh g^{-1}, respectively. In Publication I, Mg was reported to occupy Co site in LCO. As discussed previously in chapter 4.1, the Mg^{2+} doping added to Co site in LCO induces Co^{3+} oxidization to electrochemically inactive Co^{4+}. This and the replacement of Co with the dopant atoms most likely explain the slight decrease in capacity when Mg doping is added. In case of Mg-Ti doping in Publication II, 20% of the Mg was reported to occupy the unoccupied Li site while the rest occupied the Co site similarly to Publication I. When Mg occupies both Li and Co sites, the charge deficits created cancel each other. After this, approximately 60 % of the total added Mg then occupy the Co site affecting the valence. However, Ti^{4+} occupies the Co site too, canceling the effect of Mg^{2+} and preventing the loss of electrochemically active Co^{3+}. These differences in doping and occupations could explain why Mg-Ti doping enhances the LCO initial capacity but Mg doping does not.

EELS was measured for both Mg-doped and Mg-Ti-doped LCOs. Based on the results, a small reduction in the Co valence state is observed in Mg-Ti-doped LCO. In Publication II, this was attributed to the Ti doping. However, based on the amount of dopants detected in the compound, the effect of Ti^{4+} on the Co valence should be cancelled by Mg^{2+}. Because of this, alternative explanation for the behavior should be

considered. Interestingly, in Publication I lithiation doping of Mg was observed to induce an even Mg distribution through the particle while no change was observed in the valence state of Co measured by EELS. Ti, on the other hand, has been reported in the literature to distribute mainly on the particle surface [170]. It is therefore proposed that in lithiation-Mg-Ti-doped LCO, the Mg is evenly distributed to the structure while Ti remains close to the surface. The samples measured by TEM and EELS have to be very thin, and thus the particles selected for the EELS measurement in Publication II were typically small separated primary particles in which the surface is overrepresented. The amount of both dopants is small, and as Mg is distributed through the particle, its effect on the Co valence cannot be detected. However. Ti, which is assumed to distribute to the surface, would locally affect more Co ions and its effect on the material could thus be observed. This could explain why the effect of Ti was observed in Publication II even though stoichiometrically it should not be possible. To verify this, however, the surface composition of the Mg-Ti-doped LCO particles should be investigated.

As already mentioned, the materials were not cycled in the same voltage ranges. Mg-Ti doped LCO was cycled in the voltage ranges of 3.0–4.2 V and 3.0–4.4 V, the former inducing capacity retention of 89 % after 1000 cycles and the latter 80 % after 240 cycles. Mg-doped LCO was cycled using the voltage range of 3.0–4.3 V, and after 1000 cycles the capacity retention was 82 %. Based on the electrochemical investigations in Publication I and II, the 3.0–4.3 V range appears to be the most useful. Both the rate capability and cyclability of the material in this voltage range are good and compared to 3.0–4.2 V, higher capacity can be obtained. Therefore, it would be great to learn how the Mg-Ti-doped LCO would behave in this voltage range. If its known capacity retentions are considered, by linear approximation the Mg-Ti-doped LCO would reach SOH 80 % after 440 cycles. This is considerably poorer than the capacity retention of Mg-doped LCO in the same voltage range. However, previous literature works show that the voltage range rarely affects the cycle life linearly, instead the capacity retention drop accelerates the higher the cutoff voltage [187,188]. In addition, the cutoff voltage of 4.4 V in LCO/graphite pouch cell matches approximately the potential of 4.5 V vs Li^+/Li in which a detrimental phase transition occurs in LCO [135,187,189]. This most likely considerably reduces the capacity retention in 3.0–4.4 V, and would indicate clearly better capacity retention in 3.0–4.3 V. It is therefore quite likely that the real cycle life of Mg-Ti-doped LCO in the voltage range of 3.0–4.3 V would exceed the 440 cycles and perhaps even reach the 1000 cycles.

5. Recycling of positive electrode materials

The consumption of Li-ion batteries for consumer electronics, electric vehicles and energy storage applications is increasing rapidly. Between 2000 and 2020 it has increased by 20 times, from 500 million units to 10 billion units [190]. In the future the market is expected to grow with approximately 25 % annually [6]. This will lead to both resource shortages of several critical elements and generation of large amounts of end-of-life spent Li-ion batteries [6,10,11,190]. The spent Li-ion batteries are a significant secondary raw material resource, containing e.g. 5–30 wt% of Co, 0–10 wt% of Ni, 2–12 wt% of Li, 7–17 wt% of Cu and 3–10 wt% of Al, in addition to graphite and Fe [191]. Therefore, to answer the need for raw materials as well as to enhance the material circulation, it is important to investigate the recycling and reusing of Li-ion battery materials. However, one Li-ion battery cell consists of several components tightly tied together, and a battery pack e.g. for an electric vehicle may consists of hundreds of cells, which complicates the recycling considerably.

Several different methods, such as hydrometallurgy, pyrometallurgy and biometallurgy-based routes can be used in order to collect the wanted elements and components [181,192] in Li-ion battery waste. The hydrometallurgy-based routes, which typically consist of acid leaching, precipitation, and solvent extraction steps, generally have a high extraction and metal selectivity rates while the energy consumption is low. The disadvantages of the method include several process steps and large waste solution quatities. [164,185,193–198] Pyrometallurgy-based methods, in which the battery scraps are heated, are efficient and easy to scale up, but the high temperatures needed lead to high energy consumption and emissions [199,200]. Biometallurgy-based methods, in which bacteria is utilized in the metal extraction, are inexpensive to use but the extraction processes are slow [201–203].

In the literature, the Li-ion battery recycling investigations concentrating on active materials can be roughly divided to two categories. In the first category, all the components, such as active materials, current collectors and casing, are treated together in the metal recovery process [161,182,183,204], and in the second category, the components are first separated and then recycled [185,194,197,205–211]. The dismantling of the battery pack before the recollection has been a more popular approach in the literature. The advantage of this is that a separation process preceding the recovery greatly decreases the amount of impurities in the recovered materials. However, the separation processes can be laborious and time consuming. Because of this, processing the whole battery is often convenient, as the separation processes in the beginning are skipped. However, all the battery components in the same material flow initially increases the amount of impurities in the final recovered product and

additional process steps are necessary to reduce the impurity concentrations in the recycled material [161].

5.1 Cu impurity in Li-ion battery recycling

Hydrometallurgical techniques are promising for sustainable battery recycling. Currently, over 95 % of Co and Li can be leached out of the recycled waste using sulfuric acid and H_2O_2 [212,213]. Of this 95–98 % of Co [214] and 85–90 % of Li [215] are recoverable for reuse. However, while the recovery of Co and Li has been investigated, it is generally done using synthetic solutions or active material fractions that do not represent the real industrial battery waste. The fractions used in state-of-the-art recycling processes include all battery parts such as current collectors and casing in addition to active materials. This leads to large concentrations of elements such as Al, Cu and Fe, which will affect the active material recovery process as well as the electrochemical properties of the recovered material. E.g. removal of Fe and Al by neutralization and precipitation leads to 38 % loss of Co [196]. Complete removal of Cu from Co, Mn and Ni typically requires a multi-stage solvent extraction process and is thus challenging[216]. As a summary, the total recovery of Co and Li is challenging and recovered products might still contain impurities originating from the crushed batteries. Therefore, investigating the effect of impurities in the recycling processes is important and understanding throughout the whole process is needed. To answer this need, in Publication III, Li_2CO_3 and $CoSO_4$ were recovered from real Li-ion battery waste using a hydrometallurgical process. After this, the recovered products were used to synthesize $LiCoO_2$ and the effect of impurity Cu on the electrochemical performance was investigated.

The Li-ion battery waste fraction used in the work contained 23.6 % Co, 6.2 % Cu, 3.7 % Li and smaller amounts of Ni, Al, Mn and Fe. The leaching was done using 2 M H_2SO_4 and 5 vol% H_2O_2 and the extractions were ca. 98 % for Co and Li and 69 % for Cu. To recover Co and Li, the leaching solution was subjected to the series of unit processes. These included Fe and Al removal using Di-(2-ethylhexyl) phosphoric acid, Cu removal by precipitation, Co recovery using Cynaex 272, stripping and crystallization, Ni removal by precipitation and Li recovery by carbonation and evaporation, in this order. The Co recovery with Cynaex was repeated five times to simulate the process in industry and to obtain good Co extraction. The first two batches contained high level of impurities and were mixed together to form $CoSO_4$ #1 (Cu 3.5 %) and the last three batches together to form $CoSO_4$ #2 with lower impurity level (Cu 0.5 %). After the recoveries, the obtained $CoSO_4$·nH2O salts were heat-treated to obtain two Co_3O_4s, which were subsequently mixed and heated with the recycled Li_2CO_3 to produce two $LiCoO_2$s, one with high Cu concentration (91.5 mg g^{-1}) and the other with low Cu concentration (4.8 mg g^{-1}). In addition to Cu, both materials contained other impurities as well, most notably 46.2 mg g^{-1} (Cu-rich LCO) and 3.3 mg g^{-1} (low-Cu LCO) of Mn.

The electrochemical performance of the recovered materials was investigated with CV, and the results are collected in Figure 12. The peak separations are 53 mV, 68 mV and 102 mV for Cu-rich, low-Cu and reference LCOs, respectively, indicating that the Cu-rich LCO has the lowest resistance, whereas the reference LCO has the largest. Similarly, the peak intensity and width varies, and interestingly, the cathodic peak of low-Cu LCO is considerably sharper than the two others, indicating that Li can be

inserted back to the structure more easily. This is in agreement with previous studies that showed that the Li diffusion is increased by the presence of Cu in LCO [217].

Rate capability of the recycled LCOs (Figure 12b) was investigated to observe their performance at different currents. The charge capacities of the investigated materials are 166 mAh g^{-1}, 148 mAh g^{-1} and 163 mAh g^{-1}, for reference, Cu-rich and low-Cu LCOs, respectively. The lower capacities of the recycled LCOs are concluded to be caused by the electrochemically inactive Cu within the materials. Interestingly, the charge capacity of low-Cu LCO is affected quite a little. The discharge capacities of the materials are 160 mAh g^{-1}, 128 mAh g^{-1} and 147 mAh g^{-1}, for reference, Cu-rich and low-Cu LCOs, respectively, which shows that the Coulombic efficiency of the recycled materials during the first cycle is poor and cyclable Li is lost. However, while at low currents the recycled materials perform poorer than the reference, at high C-rates this is reversed with both recycled samples showing enhanced rate capability, the low-Cu LCO performing the best. As the capacity drop from 0.03C to 5.0C is similar for both low-Cu and Cu-rich LCOs, the better rate capability of low-Cu LCO compared to Cu-rich LCO is most likely due to the different Coulombic efficiencies of the samples during the formation cycle.

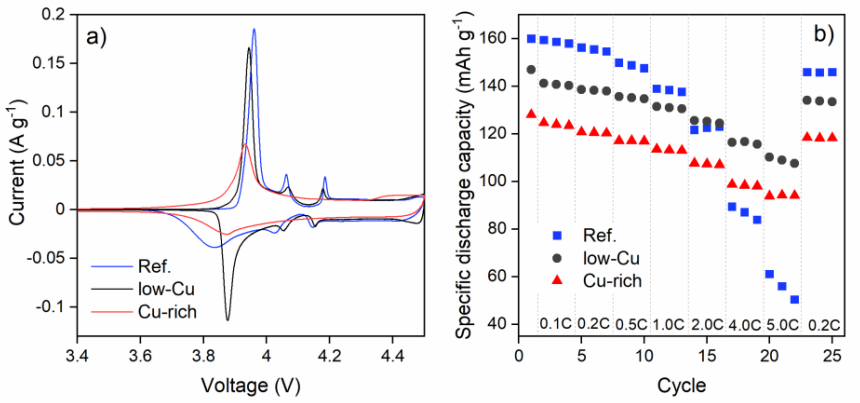

Figure 12. Electrochemical performance of the recovered LCOs in half-cells. a) Cyclic voltammograms in the voltage range of 3.0–4.5 V, and b) rate capability in the voltage range of 3.0–4.3 V.

The cycling results (Figure 13) show that both recycled materials have enhanced cyclability compared to the reference LCO. The improvement is attributed to the suppression of the charge-transfer resistance (mid-frequency semicircle) in both samples. This, in addition with the CV results, suggests that the Cu impurity enhances the charge transfer in the sample. While the cyclability of the Cu-rich LCO is better than low-Cu LCO's, due to the higher starting capacity of low-Cu LCO, after 50 cycles it still has the highest capacity. Thus, the charge-transfer resistance of low-Cu LCO is also smaller. As both CV and rate capability results indicate that low-Cu LCO performs the best, the good cyclability of Cu-rich LCO is a slight surprise. However, as the elemental analysis showed, the Cu-rich LCO contains also a considerable amount of Mn. Mn is typically used as a stabilizer for layered transition metal oxides, and therefore the good cyclability of Cu-rich LCO can be attributed to it.

At the beginning cycles, the active material/current collector interphase resistances (high-frequency semicircle) of the recycled materials are larger than the reference LCO's. This is attributed to the capacity loss during the first cycle. The capacity loss is

most likely caused by the electrolyte reacting with the electrode surface and the formation of passivating layer on it. This is then seen as an increase in the interphase resistance. The especially large interphase resistance of low-Cu LCO in the beginning is attributed to the small particle size, leading to larger surface area to react with the electrolyte.

While the impurities in this work can be concluded to improve the stability of LCO, the use of the Cu has to be investigated more. Some commonly used dopant metals for positive electrodes, such as Mn and Fe, have been reported to dissolve from the positive electrode, drift to the negative electrode and have a detrimental effect on the negative electrode SEI layer upon cycling in full cells [37,218]. While Cu doping of layered transition metal oxides has been investigated before, the behavior of Cu-doped positive electrode materials during full cell cycling is not known well. The results presented in Figure 13 suggest stable behavior, but it should be considered that the cycling is done in half-cells and only for 50 cycles. In half-cells, metallic Li is used as a counter electrode instead of the graphite of a typical full cell. The composition and behavior of Li metal SEI differs from graphite SEI behavior and therefore, conclusions cannot be made based on only half-cell measurements. To verify the behavior of Cu doping, long-term cycling in full cells should be done.

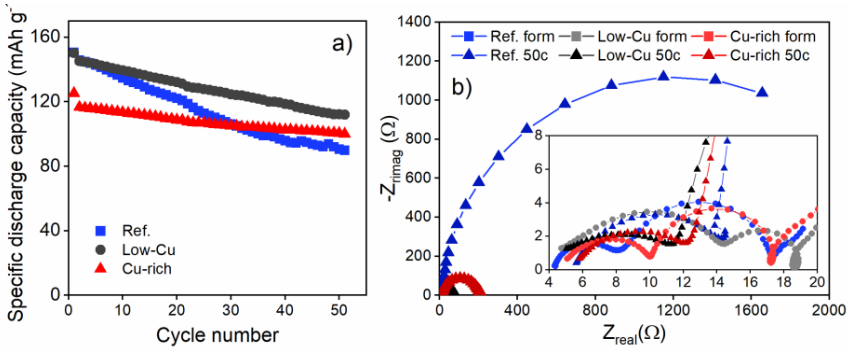

Figure 13. a) The long-term cycling and b) the Nyquist diagram of the impedance data of the recovered LCOs in three-electrode setup.

As a conclusion, in Publication III Li-ion battery waste was recycled using a hydrometallurgical method following the behavior of Li, Co and Cu. Two LCOs containing Cu impurities were synthesized using precursors obtained from the recycling process and their electrochemical properties were tested. The Co and Li recovery rates were only 89 % and 55 %, respectively, with Li lost during the solvent extraction and evaporation processes and Co in neutralization-precipitation stage. The residual Cu was extracted together with Co, and this resulted in contamination of the $CoSO_4$ product. The presence of impurity Cu decreased the initial capacity of the synthesized LCOs but improved both the rate performance and long-term cycling of the materials. The role of Cu was therefore concluded to be two-fold offering both disadvantageous and advantageous properties.

5.2 Reuse of re-lithiated aged LCO electrodes

While metals can be recovered well with several methods nowadays, the typical layered structure of the metal oxide intercalation compounds is almost certainly lost,

and the material downgraded. During the recycling process, the positive electrode materials are generally reduced to lower value chemicals, e.g. precursors such as $CoSO_4$ [161,183,185,193,219], $Co(OH)_2$ [194,205,220], $CoCO_3$ [181,182], and Li_2CO_3 [161,185,193,194,219,220], and energy is required to synthesize these compounds back to electrode materials. However, *post mortem* studies of battery electrodes have shown that a large part of the positive electrode aging is caused by loss of Li to the negative electrode, and the layered structure is not destroyed [146]. Therefore, it would be convenient if this original electrode material structure could be spared during recycling. Similarly, the removal and reapplying of the active material from the current collector leads to back-and-forth steps in recycling, and thus reactivating the electrode material without removing it from the current collector is an interesting topic. Recently, the reactivation of LCO has been investigated by a few groups [179,180,221] but in all these studies, LCO was at some point removed from the current collector. Therefore, in Publication IV the electrochemical re-lithiation of aged LCO electrode was investigated without removing the active material from the current collector.

Two different LCOs, stoichiometric $LiCoO_2$ (S-LCO) and Mg-Ti-doped $LiCoO_2$ (D-LCO) were investigated in this work. Based on the ICP-OES studies, the Li/Co ratio was slightly below 1 for both samples and D-LCO contained 0.5 mol-% Mg and 0.2 mol-% Ti. The aged electrodes were collected from aged LCO/graphite pouch cells cycled in the voltage range of 3.0–4.4 V. SOH of 70 %, which is lower than the typically used end-of-life SOH of 80%, was selected for the re-lithiation tests to investigate could these slightly over-aged cells still be revived. The number of cycles required to reach SOH 70 % varied between cells and depended on the material, being 50–100 cycles for S-LCO and 250–300 cycles for D-LCO. After the targeted SOH was reached, the cells were discharged, disassembled and the investigated electrodes collected and washed with DMC. The collected electrodes were then assembled to new half-cells in which they were electrochemically re-lithiated. The re-collection process is illustrated in Figure 14.

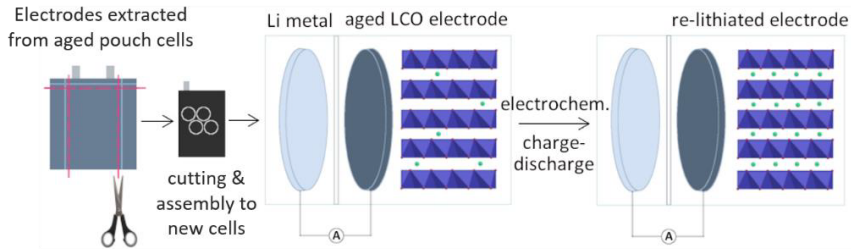

Figure 14. The electrode collection and re-lithiation process.

The structural changes caused by aging and re-lithiation were investigated with XRD, Raman spectroscopy, EELS and SEM. As the XRD patterns in Figure 15 show, the lattice structure of $LiCoO_2$ is observed to change upon cycling. The initial rhombohedral structure in hexagonal setting (H1) is observed to change to a similar but expanded structure (H2) when the material is aged, the amount of H2 increasing and H1 decreasing with prolonged aging. After the aged electrode is re-lithiated, however, the H2 phase is observed to disappear and the H1 to be formed again, which indicates that the original structure of the material is regained and the re-lithiation is successful.

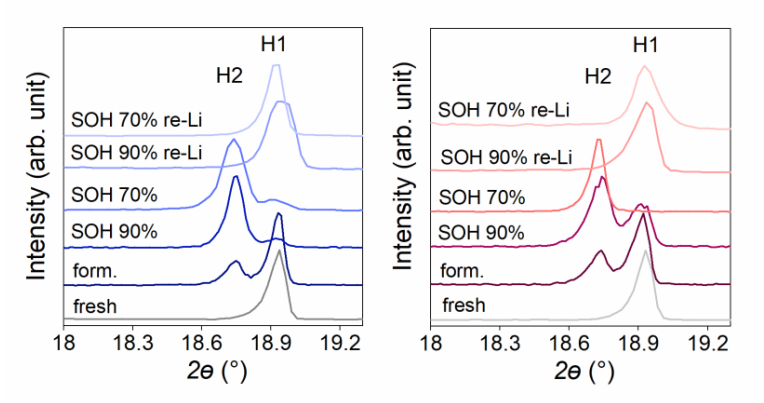

Figure 15. Magnification of the XRD patterns of the fresh, formatted, aged, and re-lithiated S-LCOs and D-LCOs near the divided (003) reflection at 18.6–19.0°.

The re-lithiation can also be verified from the electrochemical results. After the electrodes were extracted from the pouch cell and assembled to half-cells, the half-cells were charged and discharged with a 0.1 C current to perform the re-lithiation. In CV results presented in Figure 16, the first cycle represents this, and the first charge capacity equals to the remaining usable Li in the aged electrode. The second CV cycle represents the result of the re-lithiation.

The typical Li insertion and extraction peaks for $LiCoO_2$ caused by two-phase domain and Li ordering from rhombohedral to monoclinic and back are observed for both stoichiometric and Mg-Ti-doped LCOs. The peaks for aged electrodes are wider than for fresh samples, which indicates that the resistance of the electrodes increases during cycling. In addition, the first lithiation peak after aging is clearly lower than the second peak. The material capacities are calculated to increase from 104 mAh g^{-1} to 180 mAh g^{-1} for S-LCO and from 120 mAh g^{-1} to 180 mAh g^{-1} for D- LCO, indicating the recovery of the lost capacity. In other words, the LCO materials can be electrochemically re-lithiated using a metallic Li as a counter electrode. This in turn suggests that the biggest cause for capacity loss in these materials is loss of Li, and it is supported by the AAS results showing increasing amount of Li in the aged graphite electrodes.

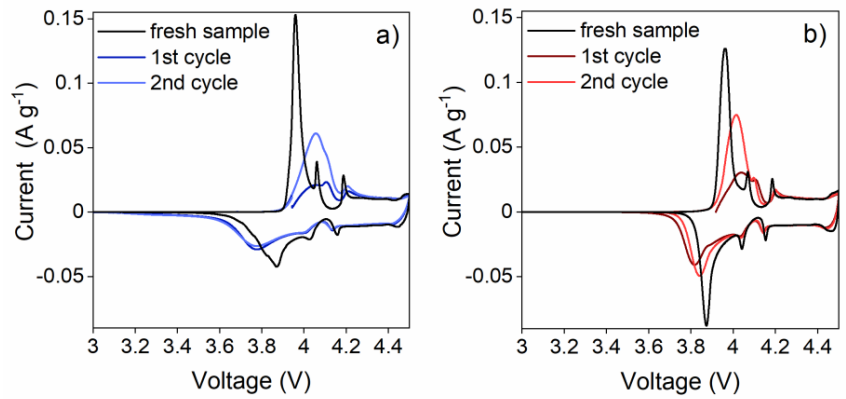

Figure 16. The CV plots of the re-lithiated a) S-LCO and b) D-LCO at SOH 70 % in the voltage range of 3.0–4.5 V compared to the CV plots of the fresh samples.

Based on the successful electrochemical re-lithiation shown in Figure 16, the reuse of the re-lithiated electrodes was investigated. The electrodes recovered after aging to SOH 70 % were cycled in half-cells using the voltage range of 3.0–4.5 V and the C-rate of 0.5C and the performance compared to fresh electrodes is presented in Figure 17. The capacity retention of D-LCO is observed to be much better compared to S-LCO for both fresh and re-lithiated electrodes. After 50 cycles the specific capacity of re-lithiated D-LCO is 125 mAh g^{-1} while it is 0 mAh g^{-1} for re-lithiated S-LCO. The cyclability of the re-lithiated materials is observed to be only slightly poorer than those of the fresh materials. For example, after 50 cycles, the capacity retentions of fresh and re-lithiated D-LCOs are 86 % and 83 %, which is a promising result from recycling perspective considering the high cut-off voltage used in the cycling.

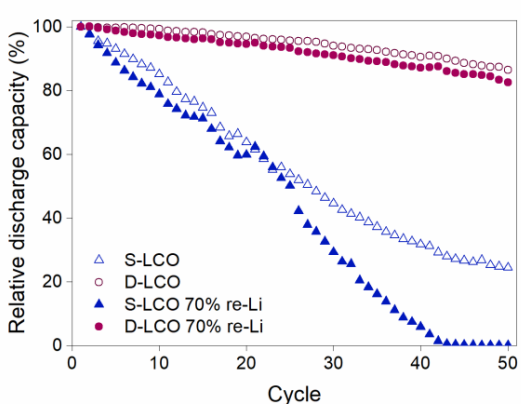

Figure 17. Cycle life of the re-lithiated LCOs aged to SOH 70 % compared to the fresh materials. The measurements were performed in half-cells using voltage range of 3.0–4.5 V.

The impedance spectra presented in Figure 18a and 18b expose two factors contributing to the cyclability of the re-lithiated electrodes. First, the active material/current collector interphase resistance (the high frequency semicircle) is observed to be larger for re-lithiated electrodes than for fresh electrodes cycled similar number of cycles. This indicates that during initial cycling a change occurs in the particle surface that is not restored in re-lithiation. It is speculated that this could be caused by either the degradation of binder and conductive carbon or loosening contact between LCO particles and the current collector, both leading to decrease in conductivity and thus increase in the active material/current collector resistance. This is, however, difficult to verify due to the mixed composition of the electrode. Either of these would nevertheless explain the broadening of the CV peaks observed in Figure 16.

The second factor affecting the cyclability of the re-lithiated electrodes is the changes observed in the charge-transfer resistances (mid-frequency semicircle). The charge-transfer resistance of the re-lithiated electrodes increases with cycling, the increase being much larger for S-LCO than for D-LCO. The slower charge-transfer resistance increase in fresh electrodes is attributed to Mg and Ti doping in Publication II, and the same process is considered to be behind the increase for re-lithiated electrodes. The rate of increase, however, is larger for re-lithiated electrodes. Only 10 cycles after the re-lithiation, the mid-frequency semicircle of the S-LCO is huge compared to the fresh electrode. For D-LCO the difference between the fresh and re-lithiated

electrodes after 50 cycles is not excessively large. The difference between stoichiometric and Mg-Ti-doped LCOs is attributed to changes in the stacking order during the cycling. While the stacking orders of both materials decrease upon aging if fresh and re-lithiated samples are compared, the decrease is larger for stoichiometric LCO indicating that the initial structure is not restored as well. The more unordered lattice structure leads to increase in resistance.

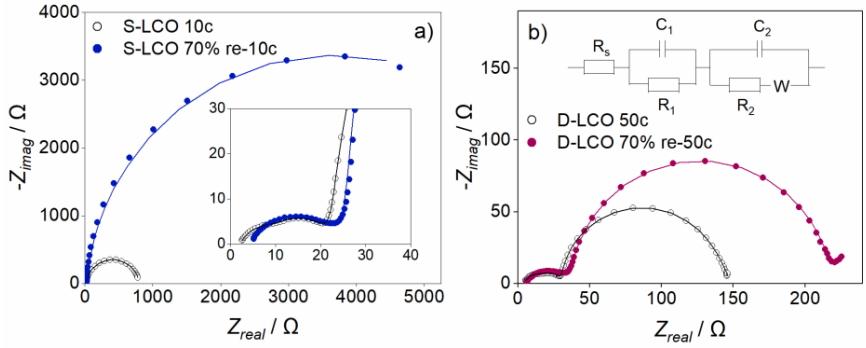

Figure 18. The Nyquist diagrams of the fresh and the re-lithiated LCOs cycled a certain number of cycles. a) stoichiometric LCO after 10 cycles, b) Mg-Ti-doped LCO after 50 cycles. The measurements were performed in three-electrode cells cycled in the voltage range of 3.0–4.5 V at the SOC of 50 %. Experimental data is presented as dots and fitted data based on the equivalent circuit as lines.

As a conclusion, it was shown that aged LCO electrodes could be electrochemically re-lithiated and that the electrochemical performance of the re-lithiated electrodes is closely related to the performance of the fresh electrodes. The factors affecting the aging become more prominent during the second aging leading to faster degradation of material performing poorly initially. The re-lithiated Mg-Ti-doped LCO performs well in electrochemical testing, the performance reaching almost the performance of the fresh electrode.

6. Conclusions

In this thesis, the effect doping on the different stages of layered transition metal oxide material life is investigated. The topic is especially scrutinized through cycle life and recycling of the materials, which are major factors to consider while improving the Li-ion battery sustainability.

First, the effect of doping and doping stage on the synthesized particles was investigated. Lithiation doping was found to have a cyclability enhancing effect on $LiCoO_2$ particles while precursor doping had a cyclability decreasing effect. The good performance of the lithiation doped samples was attributed to enhanced morphology and even Mg distribution in the particles, while in the precursor doped samples most of the Mg was distributed on the surface and the Li/Co ratio was poor. The maximum Co valence state was observed to decrease upon cycling, and the amount of decrease could be linked to the SOH of the cells. In addition to Mg doping, dual doping with Mg and Ti during lithiation step was investigated as well. Similarly to Mg doping, it was observed to improve the $LiCoO_2$ performance due to the enhanced morphology, but in addition, Ti was observed to decrease Co valence state and increase the electric conductivity of the sample. Furthermore, where the initial capacity of $LiCoO_2$ decreased upon Mg doping, the capacity increased with Mg-Ti doping. This is attributed to the valences of Ti^{4+} and Mg^{2+} cancelling each other and not reducing the amount of electrochemically available Co^{3+} while in Mg-doped $LiCoO_2$ part of the Co^{3+} is oxidized to nonreacting Co^{4+}. Both Mg doping and Mg-Ti-doping were observed to improve the cycle life of $LiCoO_2$ when applied during a lithiation step. A long cycle life increases the total energy stored in the material and decreases the energy and cost per energy produced. Lithiation doping can thus be concluded to be a very suitable method for improving the sustainability of $LiCoO_2$. While the exact effect of doping stage and dual doping on other layered transition metal oxides should be investigated separately, investigations performed here for $LiCoO_2$ can be used as a base in understanding the effect of doping in other materials.

To understand the effect of excess Li on the cycle life of $LiCoO_2$, both doped and non-doped $LiCoO_2$s were investigated with the Li/Co ratio > 1. The results were somewhat contradictory. Upon cycling of $LiCoO_2$/graphite pouch cells in the voltage ranges of 3.0–4.2 V and 3.0–4.3 V, the Li excess was observed to decrease the cyclability of non-doped and precursor-doped $LiCoO_2$s. However, it did not affect the cyclability of lithiation-doped $LiCoO_2$, and in the voltage range of 3.0–4.4 V the Li excess improved the performance of non-doped $LiCoO_2$ slightly. The excess Li was observed to induce poor stacking order, and this was concluded to be one of the causes for the faster capacity decrease of the Li-rich materials. However, as this does not explain the performance at 3.0–4.4 V, the matter should be further investigated.

To answer the growing demand for raw materials for Li-ion batteries and to protect the environment from harmful chemicals, recycling processes of Li-ion batteries must be enhanced and understood better. In Publication III, the effect of Cu impurity on the recycling of Li-ion battery waste and the electrochemical performance of $LiCoO_2$ synthesized from the recycled materials was investigated. The presence of impurity Cu decreased the initial capacity of the synthesized $LiCoO_2$s but improved both the rate capability and cycle life of the materials. Therefore, the role of Cu was concluded to be two-fold, producing both disadvantages and advantages. Currently, the state-of-the-art industrial processes aim to produce extremely pure metallic salt precursors that can be doped afterwards in the synthesis of the active materials. However, some of the impurities in the recycling process may be beneficial for the active material performance, and not a disadvantage as is currently often thought. If the effect of impurities was understood, certain impurity metals could be left in with the collected metal, which could lead to a reduction in separation steps. Simultaneously however, the addition of dopants in early synthesis stages should be considered carefully, because as shown in Publication I, it does not always have a beneficial effect on the electrochemical performance. Considering the lowered initial capacity of Cu-containing recycled $LiCoO_2$s in Publication III, their use in real-life applications would most likely be quite limited even though the performance is otherwise good. Therefore, while the utilized hydrometallurgical process was proved to work and provide extraction rates comparable to literature, it should be investigated more to fully understand the effects of different steps on the final product and the amount impurities in it. An alternative to consider as well is the separation of the basic parts of Li-ion battery in the beginning of recycling to avoid impurities in recycled chemicals. This would increase the number of process steps in the beginning but reduce them at the leaching stage and decrease the risk of contamination in all recollected fractions as mixing of components is prevented.

Many state-of-the-art recycling methods consists of several process steps that consume both energy and chemicals. In addition, the recycled product is often downgraded to less valuable chemical compared to the initial recycled compound. In Publication IV, a new method to regenerate spent Li-ion battery positive electrode materials by electrochemical re-lithiation was presented to decrease the amount of separation steps needed in the active material recovery. The performance of the aged re-lithiated electrodes was observed to be similar to the fresh electrodes, the re-lithiated Mg-Ti-doped $LiCoO_2$ performing notably better than the reference $LiCoO_2$. This indicated that the initial performance of the material has a clear effect on how it behaves after regeneration. The aging mechanisms of the materials were observed to become more prominent during the second cycling, which lowered the cyclability of the materials slightly. However, the Mg-Ti doped $LiCoO_2$ retained its stacking order better than the reference $LiCoO_2$, which was concluded to explain the difference between the materials. The degradation of the electrode additives was also considered. The slightly lowered performance of the re-lithiated electrodes would likely restrict their use in the most demanding applications, but they were determined to be eligible for stationary energy storage in renewable energy production.

This thesis focuses on the recycling of Li-ion battery chemicals back to Li-ion battery use. However, many typical battery metals are used in other applications as well. For example, cobalt is used also in super alloys, hard metals, ceramics, and pigments [222] and nickel in stainless steel [223]. Therefore, it has to be considered, whether the waste

batteries should be recycled to precursors usable for several applications or should the recycling process steps be minimized, and the materials kept in Li-ion battery circulation. Economical pros and cons of both strategies of course affect the decision, but the environmental aspects should be considered as well. The traceability of the materials in Li-ion batteries should also be enhanced. It would enable tracking the materials from the cell preparation to the end-of-life allowing us to know e.g., what are the active electrode materials used in the cell [224,225]. This would improve the sorting and recycling of the materials.

References

[1] M. S. Whittingham, *Science* **1976**, *192*, 1126–1127.

[2] K. Mizushima, P. C. Jones, P. J. Wiseman, J. B. Goodenough, *Mater. Res. Bull.* **1980**, *15*, 783–789.

[3] A. Yoshino, K. Sanechika, T. Nakajima, *Secondary Battery*, **1985**, USP4,668,595.

[4] T. Nagaura, K. Tazawa, *Prog. Batter. Sol. Cells* **1990**, *209*, 9.

[5] "Nobel prize in Chemistry 2019," can be found under https://www.nobelprize.org/prizes/chemistry/2019/press-release/, **2019**, accessed 12.10.2021.

[6] *Global Battery Alliance & World Economic Forum: A Vision for a Sustainable Battery Value Chain in 2030 Unlocking the Full Potential to Power Sustainable Development and Climate Change Mitigation*, **2019**.

[7] J. Deng, C. Bae, A. Denlinger, T. Miller, *Joule* **2020**, *4*, 511–515.

[8] "USABC Goals for Advanced High-performance Batteries for Electric Vehicle (EV) Applications," can be found under https://www.uscar.org/guest/article_view.php?articles_id=85, **2020**, accessed 12.10.2021.

[9] H. C. Hesse, M. Schimpe, D. Kucevic, A. Jossen, *Energies* **2017**, *10*, DOI 10.3390/en10122107.

[10] J. Bobba, S. Carrara, J. Huisman, F. Mathieux, C. Pavel, *Critical Raw Materials for Strategic Technologies and Sectors in the EU A Foresight Study by European Commission*, **2020**.

[11] D. J. Garole, R. Hossain, V. J. Garole, V. Sahajwalla, J. Nerkar, D. P. Dubal, *ChemSusChem* **2020**, *13*, 3079–3100.

[12] J. Heelan, E. Gratz, Z. Zheng, Q. Wang, M. Chen, D. Apelian, Y. Wang, *Jom* **2016**, *68*, 2632–2638.

[13] D. Linden, T. B. Reddy, *HANDBOOK OF BATTERIES*, McGraw-Hill Companies, Inc., United States of America, **1999**.

[14] J. B. Goodenough, K. S. Park, *J. Am. Chem. Soc.* **2013**, *135*, 1167–1176.

[15] S. Goriparti, E. Miele, F. De Angelis, E. Di Fabrizio, R. Proietti Zaccaria, C. Capiglia, *J. Power Sources* **2014**, *257*, 421–443.

[16] J. N. Reimers, J. R. Dahn, *J. Electrochem. Soc.* **1992**, *139*, 2091–2097.

[17] J. R. Dahn, E. W. Fuller, M. Obrovac, U. von Sacken, *Solid State Ionics* **1994**, *69*, 265–270.

[18] S. Venkatraman, Y. Shin, A. Manthiram, *Electrochem. Solid-State Lett.* **2003**, *6*, 6–10.

[19] C. B. L. Nkulu, L. Casas, V. Haufroid, T. De Putter, N. D. Saenen, T. Kayembe-Kitenge, P. M. Obadia, D. K. W. Mukoma, J. M. L. Ilunga, T. S. Nawrot, O. L. Numbi, E. Smolders, B. Nemery, *Nat. Sustain.* **2018**, *1*, 495–504.

[20] B. K. Sovacool, *Extr. Ind. Soc.* **2019**, *6*, 915–939.

[21] N. Nitta, F. Wu, J. T. Lee, G. Yushin, *Mater. Today* **2015**, *18*, 252–264.

[22] A. Rougier, P. Gravereau, C. Delmas, *J. Electrochem. Soc.* **1996**, *143*, 1168–1175.

[23] G. Vitins, K. West, *J. Electrochem. Soc.* **1997**, *144*, 2587–2592.

[24] N. Yabuuchi, T. Ohzuku, *J. Power Sources* **2003**, *119–121*, 171–174.

[25] A. M. Kannan, A. Manthiram, *J. Electrochem. Soc.* **2003**, *150*, A349.

[26] H. Kobayashi, Y. Arachi, S. Emura, H. Kageyama, K. Tatsumi, T. Kamiyama, *J. Power Sources* **2005**, *146*, 640–644.

[27] A. Manthiram, *Nat. Commun.* **2020**, *11*, 1–9.

[28] J. Xu, F. Lin, M. M. Doeff, W. Tong, *J. Mater. Chem. A* **2017**, *5*, 874–901.

[29] S. Bak, E. Hu, Y. Zhou, X. Yu, S. D. Senanayake, S. Cho, K. Kim, K. Y. Chung, X. Yang, K. Nam, *Appl. Mater. Interfaces* **2014**, *6*, 22594–22601.

[30] S. S. Zhang, *Energy Storage Mater.* **2020**, *24*, 247–254.

[31] Y. Itou, Y. Ukyo, *J. Power Sources* **2005**, *146*, 39–44.

[32] G. E. Blomgren, *J. Electrochem. Soc.* **2017**, *164*, A5019–A5025.

[33] Z. Lu, J. R. Dahn, *J. Electrochem. Soc.* **2002**, *149*, A815.

[34] M. M. Thackeray, S. H. Kang, C. S. Johnson, J. T. Vaughey, R. Benedek, S. A. Hackney, *J. Mater. Chem.* **2007**, *17*, 3112–3125.

[35] M. M. Thackeray, *Prog. Solid State Chem.* **1997**, *25*, 1–71.

[36] J. Tu, X. B. Zhao, G. S. Cao, D. G. Zhuang, T. J. Zhu, J. P. Tu, *Electrochim. Acta* **2006**, *51*, 6456–6462.

[37] M. Wohlfahrt-Mehrens, C. Vogler, J. Garche, *J. Power Sources* **2004**, *127*, 58–64.

[38] M. Li, J. Lu, Z. Chen, K. Amine, *Adv. Mater.* **2018**, *30*, 1–24.

[39] A. K. Padhi, K. S. Nanjundaswamy, J. B. Goodenough, *J. Electrochem. Soc.* **1997**, *144*.

[40] A. S. Andersson, J. O. Thomas, B. Kalska, L. Häggström, *Electrochem. Solid-State Lett.* **2000**, *3*, 66–68.

[41] A. S. Andersson, J. O. Thomas, *J. Power Sources* **2001**, *97*, 498–502.

[42] A. Yamada, S. C. Chung, K. Hinokuma, *J. Electrochem. Soc.* **2001**, *148*, A224.

[43] P. S. Herle, B. Ellis, N. Coombs, L. F. Nazar, *Nat. Mater.* **2004**, *3*, 147–152.

[44] S. Y. Chung, J. T. Bloking, Y. M. Chiang, *Nat. Mater.* **2002**, *1*, 123–128.

[45] I. Carrilero, M. González, D. Anseán, J. C. Viera, J. Chacón, P. G. Pereirinha, *Transp. Res. Procedia* **2018**, *33*, 195–202.

[46] W. Xu, J. Wang, F. Ding, X. Chen, E. Nasybulin, Y. Zhang, J. G. Zhang, *Energy Environ. Sci.* **2014**, *7*, 513–537.

[47] X. Q. Zhang, X. B. Cheng, Q. Zhang, *Adv. Mater. Interfaces* **2018**, *5*, 1–19.

[48] A. Manthiram, X. Yu, S. Wang, *Nat. Rev. Mater.* **2017**, *2*, 1–16.

[49] N. A. Kaskhedikar, J. Maier, *Adv. Mater.* **2009**, *21*, 2664–2680.

[50] J. R. Dahn, *Phys. Rev. B* **1991**, *44*, 9170–9177.

[51] M. Fleischhammer, T. Waldmann, G. Bisle, B. I. Hogg, M. Wohlfahrt-Mehrens, *J. Power Sources* **2015**, *274*, 432–439.

[52] C. Uhlmann, J. Illig, M. Ender, R. Schuster, E. Ivers-Tiffée, *J. Power Sources* **2015**, *279*, 428–438.

[53] T. Waldmann, B. I. Hogg, M. Wohlfahrt-Mehrens, *J. Power Sources* **2018**, *384*, 107–124.

[54] M. Winter, J. O. Besenhard, M. E. Spahr, P. Novák, *Adv. Mater.* **1998**, *10*, 725–761.

[55] D. Aurbach, B. Markovsky, I. Weissman, E. Levi, Y. Ein-Eli, *Electrochim. Acta* **1999**, *45*, 67–86.

[56] E. Peled, D. Golodnitsky, C. Menachem, D. Bar-Tow, *J. Electrochem. Soc.* **1998**, *145*, 3482–3486.

[57] A. M. Andersson, K. Edström, *J. Electrochem. Soc.* **2001**, *148*, A1100.

[58] V. Eshkenazi, E. Peled, L. Burstein, D. Golodnitsky, *Solid State Ionics* **2004**, *170*, 83–91.

[59] S. Malmgren, K. Ciosek, M. Hahlin, T. Gustafsson, M. Gorgoi, H. Rensmo, K. Edström, *Electrochim. Acta* **2013**, *97*, 23–32.

[60] T. Ohzuku, A. Ueda, N. Yamamoto, *J. Electrochem. Soc.* **1995**, *142*, 1431–1435.

[61] S. Scharner, W. Weppner, P. Schmid-Beurmann, *J. Electrochem. Soc.* **1999**, *146*, 857–861.

[62] K. Zaghib, M. Simoneau, M. Armand, M. Gauthier, *J. Power Sources* **1999**, *81–82*, 300–305.

[63] A. S. Aricò, P. Bruce, B. Scrosati, J. M. Tarascon, W. Van Schalkwijk, *Nat. Mater.* **2005**, *4*, 366–377.

[64] Z. L. Xu, X. Liu, Y. Luo, L. Zhou, J. K. Kim, *Prog. Mater. Sci.* **2017**, *90*, 1–44.

[65] J. Wang, Y. C. K. Chen-Wiegart, J. Wang, *Angew. Chemie - Int. Ed.* **2014**, *53*, 4460–4464.

[66] C. K. Chan, H. Peng, G. Liu, K. McIlwrath, X. F. Zhang, R. A. Huggins, Y. Cui, *Nat. Nanotechnol.* **2008**, *3*, 31–35.

[67] B. Hertzberg, A. Alexeev, G. Yushin, *J. Am. Chem. Soc.* **2010**, *132*, 8548–8549.

[68] N. Liu, H. Wu, M. T. McDowell, Y. Yao, C. Wang, Y. Cui, *Nano Lett.* **2012**, *12*, 3315–3321.

[69] X. Zeng, M. Li, D. Abd El-Hady, W. Alshitari, A. S. Al-Bogami, J. Lu, K. Amine, *Adv. Energy Mater.* **2019**, *9*, 1–25.

[70] J. Li, S. Hwang, F. Guo, S. Li, Z. Chen, R. Kou, K. Sun, C. J. Sun, H. Gan, A. Yu, E. A. Stach, H. Zhou, D. Su, *Nat. Commun.* **2019**, *10*, DOI 10.1038/s41467-019-09931-2.

[71] M. V. Reddy, G. V. Subba Rao, B. V. R. Chowdari, *Chem. Rev.* **2013**, *113*, 5364–5457.

[72] P. Poizot, S. Laruelle, S. Grugeon, L. Dupont, J. Tarascon, *Nature* **2000**, *407*, 496–499.

[73] M. Marcinek, J. Syzdek, M. Marczewski, M. Piszcz, L. Niedzicki, M. Kalita, A. Plewa-Marczewska, A. Bitner, P. Wieczorek, T. Trzeciak, M. Kasprzyk, P. Łężak, Z. Zukowska, A. Zalewska, W. Wieczorek, *Solid State Ionics* **2015**, *276*, 107–126.

[74] Q. Li, J. Chen, L. Fan, X. Kong, Y. Lu, *Green Energy Environ.* **2016**, *1*, 18–42.

[75] K. Xu, *Chem. Rev.* **2014**, *114*, 11503–11618.

[76] J. M. Tarascon, M. Armand, *Nature* **2001**, *414*, 359–67.

[77] R. C. Agrawal, G. P. Pandey, *J. Phys. D. Appl. Phys.* **2008**, *41*, DOI 10.1088/0022-3727/41/22/223001.

[78] B. Sun, J. Mindemark, K. Edström, D. Brandell, *Solid State Ionics* **2014**, *262*, 738–742.

[79] K. Murata, S. Izuchi, Y. Yoshihisa, *Electrochim. Acta* **2000**, *45*, 1501–1508.

[80] T. Famprikis, P. Canepa, J. A. Dawson, M. S. Islam, C. Masquelier, *Nat. Mater.* **2019**, *18*, 1278–1291.

[81] C. Fasciani, S. Panero, J. Hassoun, B. Scrosati, *J. Power Sources* **2015**, *294*, 180–186.

[82] X. Cheng, J. Pan, Y. Zhao, M. Liao, H. Peng, *Adv. Energy Mater.* **2018**, *8*, 1–16.

[83] M. Armand, F. Endres, D. R. MacFarlane, H. Ohno, B. Scrosati, *Nat. Mater.* **2009**, *8*, 621–629.

[84] A. Lewandowski, A. Świderska-Mocek, *J. Power Sources* **2009**, *194*, 601–609.

[85] Y.-H. Chen, C.-W. Wang, G. Liu, X.-Y. Song, V. S. Battaglia, A. M. Sastry, *J. Electrochem. Soc.* **2007**, *154*, A978.

[86] X. M. Liu, Z. dong Huang, S. woon Oh, B. Zhang, P. C. Ma, M. M. F. Yuen, J. K. Kim, *Compos. Sci. Technol.* **2012**, *72*, 121–144.

[87] O. S. Medvedev, Q. Wang, A. A. Popovich, P. A. Novikov, *Ionics* **2020**, *26*, 4277–4286.

[88] S. N. Eliseeva, R. V. Apraksin, E. G. Tolstopjatova, V. V. Kondratiev, *Electrochim. Acta* **2017**, *227*, 357–366.

[89] J. Chong, S. Xun, H. Zheng, X. Song, G. Liu, P. Ridgway, J. Q. Wang, V. S. Battaglia, *J. Power Sources* **2011**, *196*, 7707–7714.

[90] G. Liu, H. Zheng, V. Battaglia, A. S. Simens, A. M. Minor, X. Song, *ECS Trans.* **2019**, *6*, 45–56.

[91] D. Versaci, R. Nasi, U. Zubair, J. Amici, M. Sgroi, M. A. Dumitrescu, C. Francia, S. Bodoardo, N. Penazzi, *J. Solid State Electrochem.* **2017**, *21*, 3429–3435.

[92] A. Magasinski, B. Zdyrko, I. Kovalenko, B. Hertzberg, R. Burtovyy, C. F. Huebner, T. F. Fuller, I. Luzinov, G. Yushin, *ACS Appl. Mater. Interfaces* **2010**, *2*, 3004–3010.

[93] B. Lestriez, S. Bahri, I. Sandu, L. Roué, D. Guyomard, *Electrochem. commun.* **2007**, *9*, 2801–2806.

[94] Z. Wang, N. Dupré, A. C. Gaillot, B. Lestriez, J. F. Martin, L. Daniel, S. Patoux, D. Guyomard, *Electrochim. Acta* **2012**, *62*, 77–83.

[95] J. Li, R. B. Lewis, J. R. Dahn, *Electrochem. Solid-State Lett.* **2007**, *10*, 6–10.

[96] J. Yang, P. Li, F. Zhong, X. Feng, W. Chen, X. Ai, H. Yang, D. Xia, Y. Cao, *Adv. Energy Mater.* **2020**, *10*, 1–10.

[97] H. Buqa, M. Holzapfel, F. Krumeich, C. Veit, P. Novák, *J. Power Sources* **2006**, *161*, 617–622.

[98] D. L. Wood, J. D. Quass, J. Li, S. Ahmed, D. Ventola, C. Daniel, *Dry. Technol.* **2018**, *36*, 234–244.

[99] A. Guerfi, M. Kaneko, M. Petitclerc, M. Mori, K. Zaghib, *J. Power Sources* **2007**, *163*, 1047–1052.

[100] X. Huang, *J. Solid State Electrochem.* **2011**, *15*, 649–662.

[101] T. H. Cho, M. Tanaka, H. Ohnishi, Y. Kondo, M. Yoshikazu, T. Nakamura, T. Sakai, *J. Power Sources* **2010**, *195*, 4272–4277.

[102] Y. Lee Min, J. W. Kim, N. S. Choi, J. Lee An, W. H. Seol, J. K. Park, *J. Power Sources* **2005**, *139*, 235–241.

[103] H. Wang, Y. Zhang, H. Gao, X. Jin, X. Xie, *Int. J. Hydrogen Energy* **2016**, *41*, 324–330.

[104] M. He, X. Zhang, K. Jiang, J. Wang, Y. Wang, *ACS Appl. Mater. Interfaces* **2015**, *7*, 738–742.

[105] S. Luiso, P. Fedkiw, *Curr. Opin. Electrochem.* **2020**, *20*, 99–107.

[106] J. Goldstei, D. Newbury, D. Joy, C. Lyman, P. Echlin, E. Lifshin, L. Sawyer, J. Michael, *Scanning Electron Microscopy and X-Ray Microanalysis*, Springer, **2003**.

[107] Z. L. Wang, *Mater. Res. Bull.* **2003**, *38*, 1781–1782.

[108] C. Van Bokhoven, Jeroen A. Lamberti, *X-Ray Absorption and X-Ray Emission Spectroscopy*, John Wiley & Sons Ltd, **2016**.

[109] Z. Németh, J. Szlachetko, É. G. Bajnóczi, G. Vankó, *Rev. Sci. Instrum.* **2016**, *87*, 103105.

[110] G. T. Seidler, D. R. Mortensen, A. J. Remesnik, J. I. Pacold, N. A. Ball, N. Barry, M. Styczinski, O. R. Hoidn, *Rev. Sci. Instrum.* **2014**, *85*, DOI 10.1063/1.4901599.

[111] A. S. Ditter, E. P. Jahrman, L. R. Bradshaw, X. Xia, P. J. Pauzauskie, G. T. Seidler, *J. Synchrotron Radiat.* **2019**, *26*, 2086–2093.

[112] A. P. Honkanen, S. Ollikkala, T. Ahopelto, A. J. Kallio, M. Blomberg, S. Huotari, *Rev. Sci. Instrum.* **2019**, *90*, DOI 10.1063/1.5084049.

[113] P. Zimmermann, S. Peredkov, P. M. Abdala, S. DeBeer, M. Tromp, C. Müller, J. A. van Bokhoven, *Coord. Chem. Rev.* **2020**, *423*, 213466.

[114] Z. L. Wang, J. S. Yin, Y. D. Jiang, *Micron* **2000**, *31*, 571–580.

[115] H. P. Kulg, L. E. Alexander, *X-Ray Diffraction Procedures for Polycrystalline and Amorphous Materials*, John Wiley & Sons, Inc., **1954**.

[116] Y. Waseda, E. Matsubara, K. Shinoda, *X-Ray Diffraction Crystallography, Introduction, Examples and Solved Problems*, Springer, **2011**.

[117] K. Nakamoto, C. W. Brown, *Introductory Raman Spectroscopy*, **1994**.

[118] R. Baddour-Hadjean, J.-P. Pereira-Ramos, *Chem. Rev.* **2010**, *110*, 1278–1319.

[119] G. A. Somorjai, *Introduction to Surface Chemistry and Catalysis*, Wiley Interscience, **1994**.

[120] N. Schweikert, H. Hahn, S. Indris, *Phys. Chem. Chem. Phys.* **2011**, *13*, 6234–6240.

[121] P. T. Kissinger, W. R. Heineman, *J. Chem. Educ.* **1983**, *60*, 702–706.

[122] W. Weppner, R. A. Huggins, *J. Electrochem. Soc.* **1977**, *124*, 1569–1578.

[123] D. W. Dees, S. Kawauchi, D. P. Abraham, J. Prakash, *J. Power Sources* **2009**, *189*, 263–268.

[124] S.-I. Pyun, Shin Heon-Cheol, Lee Jong-Wong, J.-Y. Go, *Electrochemistry of Insertion Materials for Hydrogen and Lithium*, Springer-Verlag, Berlin Heidelberg, **2012**.

[125] J. W. Fergus, *J. Power Sources* **2010**, *195*, 939–954.

[126] L. Xiao, Y. Yang, Y. Zhao, X. Ai, H. Yang, Y. Cao, *J. Solid State Electrochem.* **2008**, *12*, 149–153.

[127] J. Cho, Y. J. Kim, B. Park, *Chem. Mater.* **2000**, *12*, 3788–3791.

[128] M. R. Laskar, D. H. K. Jackson, S. Xu, R. J. Hamers, D. Morgan, T. F. Kuech, *ACS Appl. Mater. Interfaces* **2017**, *9*, 11231–11239.

[129] Y. K. Sun, Z. Chen, H. J. Noh, D. J. Lee, H. G. Jung, Y. Ren, S. Wang, C. S. Yoon, S. T. Myung, K. Amine, *Nat. Mater.* **2012**, *11*, 942–947.

[130] S. T. Myung, H. J. Noh, S. J. Yoon, E. J. Lee, Y. K. Sun, *J. Phys. Chem. Lett.* **2014**, *5*, 671–679.

[131] S. Levasseur, M. Menetrier, Y. Shao-Horn, L. Gautier, A. Audemer, G. Demazeau, A. Largeteau, C. Delmas, *Chem. Mater.* **2003**, *15*, 348–354.

[132] Z. Lu, L. Y. Beaulieu, R. A. Donaberger, C. L. Thomas, J. R. Dahn, *J. Electrochem. Soc.* **2002**, *149*, A778.

[133] S. Sharifi-Asl, J. Lu, K. Amine, R. Shahbazian-Yassar, *Adv. Energy Mater.* **2019**, *9*, DOI 10.1002/aenm.201900551.

[134] J. Yu, Z. Han, X. Hu, H. Zhan, Y. Zhou, X. Liu, *J. Power Sources* **2013**, *225*, 34–39.

[135] T. Ohzuku, A. Ueda, *J. Electrochem. Soc.* **1994**, *141*, 2972–2977.

[136] V. Pimenta, M. Sathiya, D. Batuk, A. M. Abakumov, D. Giaume, S. Cassaignon, D. Larcher, J. M. Tarascon, *Chem. Mater.* **2017**, *29*, 9923–9936.

[137] F. Zhou, X. Zhao, C. Goodbrake, J. Jiang, J. R. Dahn, *J. Electrochem. Soc.* **2009**, *156*, A796.

[138] Y. Gu, D. Chen, X. Jiao, *J. Phys. Chem. B* **2005**, *109*, 17901–17906.

[139] M. Okubo, E. Hosono, T. Kudo, H. S. Zhou, I. Honma, *Solid State Ionics* **2009**, DOI 10.1016/j.ssi.2008.06.010.

[140] W. Luo, X. Li, J. R. Dahn, *J. Electrochem. Soc.* **2010**, *157*, A782.

[141] T. J. Boyle, D. Ingersoll, T. M. Alam, C. J. Tafoya, M. A. Rodriguez, K. Vanheusden, D. H. Doughty, *Chem. Mater.* **1998**, *10*, 2270–2276.

[142] X. Zhang, W. J. Jiang, A. Mauger, Qilu, F. Gendron, C. M. Julien, *J. Power Sources* **2010**, *195*, 1292–1301.

[143] M. Okubo, E. Hosono, J. Kim, M. Enomoto, N. Kojima, T. Kudo, H. Zhou, I. Honma, *J. Am. Chem. Soc.* **2007**, DOI 10.1021/ja0681927.

[144] T. Kawamura, M. Makidera, S. Okada, K. Koga, N. Miura, J. I. Yamaki, *J. Power Sources* **2005**, *146*, 27–32.

[145] Z. Chang, Z. Chen, F. Wu, H. Tang, X. Z. Yuan, H. Wang, *Electrochem. Solid-State Lett.* **2008**, *11*, A229.

[146] T. Guan, S. Sun, F. Yu, Y. Gao, P. Fan, P. Zuo, C. Du, G. Yin, *Electrochim. Acta* **2018**, *279*, 204–212.

[147] F. H. Ning, X. Gong, F. Y. Rao, X. M. Zeng, C. Y. Ouyang, *Int. J. Electrochem. Sci.* **2016**, *11*, 1951–1959.

[148] S. H. Ju, H. C. Jang, Y. C. Kang, *Mater. Chem. Phys.* **2008**, *112*, 536–541.

[149] W. Luo, J. R. Dahn, *Electrochim. Acta* **2009**, *54*, 4655–4661.

[150] C. Julien, G. A. Nazri, A. Rougier, *Solid State Ionics* **2000**, *135*, 121–130.

[151] X. Zhu, K. Shang, X. Jiang, X. Ai, H. Yang, Y. Cao, *Ceram. Int.* **2014**, *40*, 11245–11249.

[152] A. Liu, J. Li, R. Shunmugasundaram, J. R. Dahn, *J. Electrochem. Soc.* **2017**, *164*, A1655–A1664.

[153] F. Nobili, S. Dsoke, F. Croce, R. Marassi, *Electrochim. Acta* **2005**, *50*, 2307–2313.

[154] M. Mladenov, R. Stoyanova, E. Zheheva, S. Vassilev, *Electrochem. commun.* **2001**, *3*, 410–416.

[155] S. Levasseur, M. Ménétrier, C. Delmas, *Chem. Mater.* **2002**, *14*, 3584–3590.

[156] M. V. Reddy, T. W. Jie, C. J. Jafta, K. I. Ozoemena, M. K. Mathe, A. S. Nair, S. S. Peng, M. S. Idris, G. Balakrishna, F. I. Ezema, B. V. R. Chowdari, *Electrochim. Acta* **2014**, *128*, 192–197.

[157] M. C. Rao, O. M. Hussain, *J. Alloys Compd.* **2010**, *491*, 503–506.

[158] J. Yu, Z. Han, X. Hu, H. Zhan, Y. Zhou, X. Liu, *J. Power Sources* **2014**, *262*, 136–139.

[159] S. H. Kim, C. Kim, *J. Electroceramics* **2009**, *23*, 254–257.

[160] F. Nobili, F. Croce, R. Tossici, I. Meschini, P. Reale, R. Marassi, *J. Power Sources* **2012**, *197*, 276–284.

[161] C. Peng, K. Lahtinen, E. Medina, P. Kauranen, M. Karppinen, T. Kallio, B. P.

Wilson, M. Lundström, *J. Power Sources* **2020**, *450*, DOI 10.1016/j.jpowsour.2019.227630.

[162] X.-Z. Kong, D.-L. Li, K. Lahtinen, T. Kallio, X.-Q. Ren, *J. Electrochem. Soc.* **2020**, *167*, 140545.

[163] C. N. Zaheena, C. Nithya, R. Thirunakaran, A. Sivashanmugam, S. Gopukumar, *Electrochim. Acta* **2009**, *54*, 2877–2882.

[164] M. Mladenov, R. Stoyanova, E. Zhecheva, S. Vassilev, *Electrochem. commun.* **2001**, *3*, 410–416.

[165] H. Lee, H. J. Kim, D. Kim, S. Choi, *J. Power Sources* **2008**, *176*, 359–362.

[166] Z. Wen, S. Huang, X. Yang, B. Lin, *Solid State Ionics* **2008**, *179*, 1800–1805.

[167] P. Ghosh, S. Mahanty, R. N. Basu, *Mater. Chem. Phys.* **2008**, *110*, 406–410.

[168] S. Mou, K. Huang, M. Guan, X. Ma, J. song Chen, Y. Xiang, X. Zhang, *J. Power Sources* **2021**, *505*, 230067.

[169] K. Lahtinen, T. Rauhala, S. Räsänen, E. Rautama, T. Kallio, *Electrochim. Acta* **2019**, *327*, 135012.

[170] Y. S. Hong, X. Huang, C. Wei, J. Wang, J. N. Zhang, H. Yan, Y. S. Chu, P. Pianetta, R. Xiao, X. Yu, Y. Liu, H. Li, *Chem* **2020**, *6*, 2759–2769.

[171] K. Hoang, *Phys. Rev. Mater.* **2017**, *1*, DOI 10.1103/PhysRevMaterials.1.075403.

[172] S. Gopukumar, Y. Jeong, K. B. Kim, *Solid State Ionics* **2003**, *159*, 223–232.

[173] H. Tukamoto, A. R. West, *J. Electrochem. Soc.* **1997**, *144*, 3164–3168.

[174] M. Carewska, S. Scaccia, F. Croce, S. Arumugam, Y. Wang, S. Greenbaum, *Solid State Ionics* **1997**, *93*, 227–237.

[175] M. Zhang, M. Tan, H. Zhao, S. Liu, X. Shu, Y. Hu, *Appl. Surf. Sci.* **2018**, *458*, 111–118.

[176] B. Hu, X. Lou, C. Li, F. Geng, C. Zhao, J. Wang, M. Shen, B. Hu, *J. Power Sources* **2019**, *438*, 226954.

[177] Y. Deng, T. Kang, Z. Ma, X. Tan, X. Song, Z. Wang, P. Pang, D. Shu, X. Zuo, J. Nan, *Electrochim. Acta* **2019**, *295*, 703–709.

[178] L. Wang, J. Ma, C. Wang, X. Yu, R. Liu, F. Jiang, X. Sun, *Adv. Sci.* **2019**, *6*, 1900355.

[179] L. Zhang, Z. Xu, Z. He, *ACS Sustain. Chem. Eng.* **2020**, *8*, 11596–11605.

[180] J. Yang, W. Wang, H. Yang, D. Wang, *Green Chem.* **2020**, *22*, 6489–6496.

[181] B. Wang, X. Y. Lin, Y. Tang, Q. Wang, M. K. H. Leung, X. Y. Lu, *J. Power Sources* **2019**, *436*, 226828.

[182] F. Pagnanelli, E. Moscardini, P. Altimari, T. Abo Atia, L. Toro, *Waste Manag.* **2016**, *51*, 214–221.

[183] D. Dutta, A. Kumari, R. Panda, S. Jha, D. Gupta, S. Goel, M. K. Jha, *Sep. Purif. Technol.* **2018**, *200*, 327–334.

[184] A. Porvali, M. Aaltonen, S. Ojanen, O. Velazquez-Martinez, E. Eronen, F. Liu, B. P. Wilson, R. Serna-Guerrero, M. Lundström, *Resour. Conserv. Recycl.* **2019**, *142*, 257–266.

[185] J. Nan, D. Han, X. Zuo, *J. Power Sources* **2005**, *152*, 278–284.

[186] M. Ménétrier, I. Saadoune, S. Levasseur, C. Delmas, *J. Mater. Chem.* **1999**, *9*, 1135–1140.

[187] H. Xia, L. Lu, Y. S. Meng, G. Ceder, *J. Electrochem. Soc.* **2007**, *154*, A337–A342.

[188] A. M. Kannan, L. Rabenberg, A. Manthiram, *Electrochem. Solid-State Lett.* **2003**, *6*, 16–19.

[189] G. G. Amatucci, J. M. Tarascon, L. C. Klein, *J. Electrochem. Soc.* **1996**, *143*, 1114.

[190] E. M. Sarkar, T. Sarkar, M. D. Bharadwaj, *Curr. Sci.* **2018**, *114*, 2453–2458.

[191] X. Zeng, J. Li, N. Singh, *Crit. Rev. Environ. Sci. Technol.* **2014**, *44*, 1129–1165.

[192] C. Liu, J. Lin, H. Cao, Y. Zhang, Z. Sun, *J. Clean. Prod.* **2019**, *228*, 801–813.

[193] P. Zhang, T. Yokoyama, O. Itabashi, T. M. Szuki, K. Inoue, *Hydrometallurgy* **1998**, *47*, 259–271.

[194] M. A. H. Shuva, A. Kurny, *Am. J. Mater. Eng. Technol.* **2013**, *1*, 8–12.

[195] X. Chen, T. Zhou, *Waste Manag. Res.* **2014**, *32*, 1083–1093.

[196] X. Chen, Y. Chen, T. Zhou, D. Liu, H. Hu, S. Fan, *Waste Manag.* **2015**, *38*, 349–356.

[197] L. Li, R. Chen, F. Sun, F. Wu, J. Liu, *Hydrometallurgy* **2011**, *108*, 220–225.

[198] B. Wang, X. Y. Lin, Y. Tang, Q. Wang, M. K. H. Leung, X. Y. Lu, *J. Power Sources* **2019**, *436*, 226828.

[199] A. M. Bernardes, D. C. R. Espinosa, J. A. S. Tenório, *J. Power Sources* **2004**, *130*, 291–298.

[200] T. Georgi-Maschler, B. Friedrich, R. Weyhe, H. Heegn, M. Rutz, *J. Power Sources* **2012**, *207*, 173–182.

[201] D. Mishra, D. J. Kim, D. E. Ralph, J. G. Ahn, Y. H. Rhee, *Waste Manag.* **2008**, *28*, 333–338.

[202] N. Bahaloo-Horeh, S. M. Mousavi, *Waste Manag.* **2017**, *60*, 666–679.

[203] Y. Tang, H. Xie, B. Zhang, X. Chen, Z. Zhao, J. Qu, P. Xing, H. Yin, *Waste Manag.* **2019**, *97*, 140–148.

[204] Y. Kim, M. Matsuda, A. Shibayama, T. Fujita, *Resour. Process.* **2004**, *51*, 3–7.

[205] M. Contestabile, S. Panero, B. Scrosati, *J. Power Sources* **2001**, *92*, 65–69.

[206] C. K. Lee, K. I. Rhee, *J. Power Sources* **2002**, *109*, 17–21.

[207] Z. Zhang, W. He, G. Li, J. Xia, H. Hu, J. Huang, *Int. J. Electrochem. Sci.* **2014**, *9*, 3691–3700.

[208] Y. Shi, G. Chen, Z. Chen, *Green Chem.* **2018**, *20*, 851–862.

[209] J. Yu, Y. He, Z. Ge, H. Li, W. Xie, S. Wang, *Sep. Purif. Technol.* **2018**, *190*, 45–52.

[210] X. Chen, H. Ma, C. Luo, T. Zhou, *J. Hazard. Mater.* **2017**, *326*, 77–86.

[211] Y. He, T. Zhang, F. Wang, G. Zhang, W. Zhang, J. Wang, *J. Clean. Prod.* **2017**, *143*, 319–325.

[212] L. Sun, K. Qiu, *J. Hazard. Mater.* **2011**, *194*, 378–384.

[213] L. Chen, X. Tang, Y. Zhang, L. Li, Z. Zeng, Y. Zhang, *Hydrometallurgy* **2011**, *108*, 80–86.

[214] J. Kang, G. Senanayake, J. Sohn, S. M. Shin, *Hydrometallurgy* **2010**, *100*, 168–171.

[215] C. Peng, F. Liu, Z. Wang, B. P. Wilson, M. Lundström, *J. Power Sources* **2019**, *415*, 179–188.

[216] V. Sridhar, J. K. Verma, *Miner. Eng.* **2011**, *24*, 959–962.

[217] K. Kang, G. Ceder, *Phys. Rev. B* **2006**, *74*, 1–7.

[218] D. Aurbach, B. Markovsky, G. Salitra, E. Markevich, Y. Talyossef, M. Koltypin, L. Nazar, B. Ellis, D. Kovacheva, *J. Power Sources* **2007**, *165*, 491–499.

[219] J. Hu, J. Zhang, H. Li, Y. Chen, C. Wang, *J. Power Sources* **2017**, *351*, 192–199.

[220] C. H. Jo, S. T. Myung, *J. Power Sources* **2019**, *426*, 259–265.

[221] Y. Gao, Y. Li, J. Li, H. Xie, Y. Chen, *J. Alloys Compd.* **2020**, *845*, 156234.

[222] P. Alves Dias, D. Blagoeva, C. Pavel, N. Arvanitidis, *Cobalt: Demand-Supply Balances in the Transition to Electric Mobility. EUR 29381 EN, Publications Office of the European Union, Luxembourg, 2018, ISBN 978-92-79-94311-9, Doi:10.2760/97710, JRC112285.*, **2018**.

[223] A. Elshkaki, B. K. Reck, T. E. Graedel, *Resour. Conserv. Recycl.* **2017**, *125*, 300–307.

[224] G. Riexinger, J. P. Doppler, C. Haar, M. Trierweiler, A. Buss, K. Schöbel, D. Ensling, T. Bauernhansl, *Procedia CIRP* **2020**, *93*, 125–130.

[225] E. Fan, L. Li, Z. Wang, J. Lin, Y. Huang, Y. Yao, R. Chen, F. Wu, *Chem. Rev.* **2020**, DOI 10.1021/acs.chemrev.9b00535.

Aalto-DT 33/2022

ISBN 978-952-64-0718-0 (printed)
ISBN 978-952-64-0719-7 (pdf)
ISSN 1799-4934 (printed)
ISSN 1799-4942 (pdf)

Aalto University
School of Chemical Engineering
Department of Chemistry and Materials Science
www.aalto.fi

BUSINESS + ECONOMY

ART + DESIGN + ARCHITECTURE

SCIENCE + TECHNOLOGY

CROSSOVER

DOCTORAL THESES